



HAL
open science

Sustained neural rhythms reveal endogenous oscillations supporting speech perception

Sander van Bree, Ediz Sohoglu, Matthew H Davis, Benedikt Zoefel

► To cite this version:

Sander van Bree, Ediz Sohoglu, Matthew H Davis, Benedikt Zoefel. Sustained neural rhythms reveal endogenous oscillations supporting speech perception. PLoS Biology, 2021, 19 (2), pp.e3001142. 10.1371/journal.pbio.3001142 . hal-03312707

HAL Id: hal-03312707

<https://hal.science/hal-03312707>

Submitted on 2 Aug 2021

HAL is a multi-disciplinary open access archive for the deposit and dissemination of scientific research documents, whether they are published or not. The documents may come from teaching and research institutions in France or abroad, or from public or private research centers.

L'archive ouverte pluridisciplinaire **HAL**, est destinée au dépôt et à la diffusion de documents scientifiques de niveau recherche, publiés ou non, émanant des établissements d'enseignement et de recherche français ou étrangers, des laboratoires publics ou privés.

1 **Sustained neural rhythms reveal endogenous oscillations supporting speech**
2 **perception**

3
4 **Short title:** Sustained oscillations produced by rhythmic stimulation

5
6 **Authors:** Sander van Bree^{a,b,c}, Ediz Sohoglu^{a,d}, Matthew H Davis^{a,g}, Benedikt Zoefel^{a,e,f,g,*}

7
8 **Affiliations:** ^a MRC Cognition and Brain Sciences Unit, University of Cambridge, 15 Chaucer
9 Road, Cambridge CB27EF, UK

10 ^b Centre for Cognitive Neuroimaging, University of Glasgow, Glasgow, United
11 Kingdom

12 ^c School of Psychology and Centre for Human Brain Health, University of
13 Birmingham, Birmingham B15 2TT, UK

14 ^d School of Psychology, University of Sussex, Pevensey Building, Brighton, BN1
15 9QH, UK

16 ^e Centre de Recherche Cerveau et Cognition (CerCo), CNRS UMR 5549, CHU
17 Purpan, Pavillon Baudot, 31052 Toulouse, France

18 ^f Université Toulouse III Paul Sabatier, Toulouse, France

19 ^g senior author

20 *Corresponding author (benedikt.zoefel@cnrs.fr)

21
22
23
24 **Author Contributions:** Conceptualization, M. H. D. and B. Z.; Methodology, S. v. B., E. S., M. H. D.,
25 and B. Z.; Software, B. Z.; Formal Analysis, S.v.B. and B. Z.; Investigation, S. v. B.; Visualization, M.
26 H. D. and B. Z.; Writing – Original Draft, B. Z.; Writing – Review & Editing, S. v. B., E. S., M. H. D.,
27 and B. Z.; Supervision, M. H. D. and B. Z.; Project Administration, B. Z.; Funding Acquisition, M. H.
28 D. and B. Z.

29 **Abstract**

30 Rhythmic sensory or electrical stimulation will produce rhythmic brain responses. These rhythmic
31 responses are often interpreted as endogenous neural oscillations aligned (or “entrained”) to the stimulus
32 rhythm. However, stimulus-aligned brain responses can also be explained as a sequence of evoked
33 responses, which only appear regular due to the rhythmicity of the stimulus, without necessarily
34 involving underlying neural oscillations. To distinguish evoked responses from true oscillatory activity,
35 we tested whether rhythmic stimulation produces oscillatory responses which continue after the end of
36 the stimulus. Such sustained effects provide evidence for true involvement of neural oscillations. In
37 Experiment 1, we found that rhythmic intelligible, but not unintelligible speech produces oscillatory
38 responses in magnetoencephalography (MEG) which outlast the stimulus at parietal sensors. In
39 Experiment 2, we found that transcranial alternating current stimulation (tACS) leads to rhythmic
40 fluctuations in speech perception outcomes after the end of electrical stimulation. We further report that
41 the phase relation between electroencephalography (EEG) responses and rhythmic intelligible speech
42 can predict the tACS phase that leads to most accurate speech perception. Together, we provide
43 fundamental results for several lines of research – including neural entrainment and tACS – and reveal
44 endogenous neural oscillations as a key underlying principle for speech perception.

45
46
47
48
49
50
51
52
53
54
55
56

57 **Introduction**

58 The alignment of oscillatory neural activity to a rhythmic stimulus, often termed “neural entrainment”,
59 is an integral part of many current theories of speech processing [1–4]. Indeed, brain responses seem to
60 align more reliably to intelligible than to unintelligible speech [5,6]. Similarly, rhythmic electrical
61 stimulation applied to the scalp (tACS) is assumed to “entrain” brain oscillations and has been shown
62 to modulate speech processing and perception [7–11]. Despite the prominence of entrainment theories
63 in speech research and elsewhere [1,12–14], it has been surprisingly difficult to demonstrate that
64 stimulus-aligned brain responses indeed involve endogenous neural oscillations. This is because, if each
65 stimulus in a rhythmic sequence produces a brain response, the evoked brain responses will appear
66 rhythmic as well, without necessarily involving endogenous neural oscillations. This is not only true for
67 sensory stimulation: Rhythmic behavioural effects of tACS cannot be interpreted as evidence of
68 entrained endogenous oscillations; they might simply reflect the impact of regular changes in current
69 imposed onto the brain [15].

70

71 In the present work, we provide evidence that rhythmic intelligible speech and tACS entrain endogenous
72 neural oscillations. Neural oscillations are often proposed to align their high-excitability phase to
73 important events in a rhythmic sequence so as to boost the processing of these events and enhance
74 corresponding task performance [12,13]. It is possible that such a process entails a passive, “bottom-up”
75 component during which oscillations are rhythmically “pushed” by the stimulus, similar to the regular
76 swing of a pendulum (that is, the endogenous oscillation is “triggered” by an exogenous stimulus). On
77 the other hand (and not mutually exclusive), an active, “top-down” component could adjust neural
78 activity so that it is optimally aligned with a predicted stimulus. Importantly, in both cases we would
79 anticipate that oscillatory brain responses are sustained for some time after the offset of stimulation:
80 This could be because predictions about upcoming rhythmic input are upheld, and/or neural oscillations
81 are self-sustaining and (much like a pendulum swing) will continue after the cessation of a driving input.
82 Consequently, sustained oscillatory responses produced by a rhythmic stimulus *after* the cessation of
83 that stimulus can provide evidence for entrainment of endogenous neural oscillations [16,17].

84

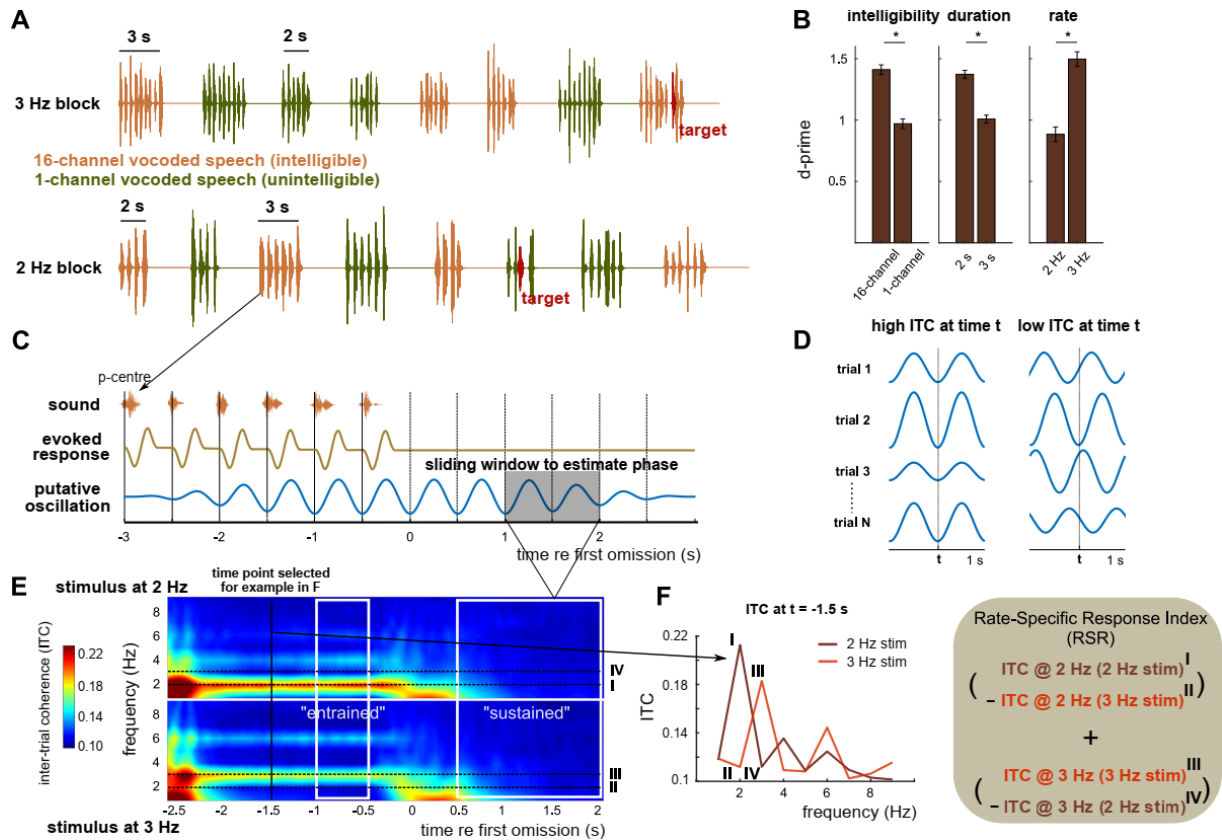
85 In this paper, we will contrast this theory of entrained oscillations with an alternative view in which
86 entrainment is merely due to responses evoked directly by the stimulus *per se*. Note that both views are
87 sufficient to accommodate existing evidence of brain signals aligned to a stimulus while the latter is
88 present. Given the difficulty of distinguishing true oscillations from other responses during rhythmic
89 input, we use the term “entrained” only to describe a signal aligned to a stimulus (irrespective of whether
90 this alignment reflects oscillations or evoked responses; see “entrainment in the broad sense” in [14]).
91 We then measure sustained rhythmic activity to infer its neural origins: Truly oscillatory activity that
92 was entrained to the rhythmic stimulus would lead to sustained rhythmic responses, but sustained
93 responses would not be expected for stimulus-evoked neural activity. In the current study, we provide
94 two distinct sources of evidence for sustained oscillatory effects: (1) oscillatory MEG responses that
95 continue after rhythmic intelligible speech and (2) oscillatory effects of tACS on speech perception that
96 continue after the termination of electrical stimulation. Furthermore, we link these two effects in single
97 participants to show how the phase of oscillatory neural responses measured with EEG can predict the
98 tACS phase at which word report is enhanced. In combination, these findings provide evidence that
99 endogenous neural oscillations in entrained brain responses play a causal role in supporting speech
100 perception.

101

102 **Results**

103 *Experiment 1: Rhythmic intelligible speech produces sustained MEG oscillations*

104 In Experiment 1, 21 participants listened to sequences of noise-vocoded [18] rhythmic speech (Fig. 1A),
105 which were 2 or 3 seconds in duration and presented at one of two different rates (2 Hz and 3 Hz).
106 Speech sequences consisted of 4, 6 or 9 one-syllable words, depending on sequence duration and speech
107 rate. These words were either clearly intelligible or completely unintelligible and noise-like, depending
108 on the number of spectral channels used during vocoding (16 or 1; see Materials and Methods).



109

110 **Figure 1. Experimental paradigm and analysis.** A. Participants listened to rhythmic speech sequences and were asked
 111 to press a button when they detected an irregularity in the stimulus rhythm (red targets). B. Performance (as d-prime)
 112 in the irregularity detection task, averaged across participants and shown for the main effects of intelligibility, duration,
 113 and rate. Error bars show standard error of mean (SEM), corrected for within-subject comparison [19]. Please refer
 114 to Data S1 for the numerical values underlying this figure panel. C. A rhythmic brain response measured during
 115 the presented sounds cannot distinguish true neural oscillations aligned to the stimulus from regular stimulus-evoked
 116 responses. However, only the oscillation-based model predicts a rhythmic response which outlasts the rhythmic
 117 stimulus. For each time point t throughout the trial, oscillatory phase was estimated based on a 1-s window centred on
 118 t (shaded grey). D. Inter-trial phase coherence (ITC) at time t is high when estimated phases are consistent across trials
 119 (left) and low otherwise (right). Note that the two examples shown differ in their 2-Hz ITC, but have similar induced
 120 power at the same frequency. E. ITC in the longer (3-s) condition, averaged across intelligibility conditions,
 121 gradiometers, and participants. Note that “time” (x-axis) refers to the centre of the 1-s windows used to estimate phase.
 122 ITC at 2 and 3 Hz, measured in response to 2 and 3 Hz sequences, were combined to form a rate-specific response index
 123 (RSR). The two time windows used for this analysis (“entrained” and “sustained”) are shown in white (results are shown
 124 in Fig. 2). F. ITC as a function of neural frequency, separately for the two stimulation rates, and for the example time
 125 point shown as a black line in E.

126

127 In a subset of trials (12.5 %), one of the words in the sequence (red in Fig. 1A) was shifted towards
 128 another (± 68 ms), and participants were given the task to detect this irregularity in the stimulus rhythm.
 129 Replicating previous work [7], performance in this task (quantified as d-prime; see Materials and
 130 Methods; Fig. 1B) was enhanced for intelligible as compared to unintelligible speech (main effect of

131 intelligibility in 3-way repeated-measures ANOVA, $F(1, 20) = 31.30$, $p < 0.0001$). We also found that
132 irregularities were easier to detect if the sequence was shorter (main effect of duration, $F(1, 20) = 32.39$,
133 $p < 0.0001$) and presented at a faster rate (main effect of rate, $F(20) = 26.76$, $p < 0.0001$; no significant
134 interactions).

135
136 Using MEG and EEG, we measured brain responses during the presented sounds and, importantly, in a
137 subsequent, silent interval of several seconds that continued until the start of the next sequence (Fig.
138 1A,C). Due to its higher signal-noise ratio, we focused our initial analyses on the MEG data. We used
139 inter-trial phase coherence (ITC) to quantify oscillatory brain responses (Fig. 1D). ITC makes use of the
140 fact that, for each of the two speech rates, the timing of the presented speech sequences (relative to the
141 “perceptual centre” of individual words, vertical lines in Fig. 1C) was identical across trials (see
142 Materials and Methods). ITC therefore has the advantage of directly testing the predicted temporal
143 evolution of the recorded signal (i.e. its phase), whereas power-based measures are focused on its
144 amplitude [20]. Fig. 1E shows ITC, separately for the two stimulus rates, and averaged across MEG
145 sensors and participants. For one example time point, Fig. 1F shows ITC as a function of neural
146 frequency.

147
148 Our hypothesis states that ITC at a given neural frequency is higher when that frequency corresponds to
149 the stimulation rate than when it does not. For example, we expect that ITC at 2 Hz during (and after)
150 the presentation of 2-Hz sequences (I in Fig. 1E,F) is higher than ITC at 2 Hz during (and after) 3-Hz
151 sequences (II in Fig. 1E,F). By comparing ITCs across the two stimulus rates (I vs II and III vs IV in
152 Fig. 1E,F), we thus developed a precise measurement of whether brain responses follow the rate of the
153 stimulus, which we term the rate-specific response index (RSR; see Materials and Methods and formula
154 in Fig. 1F). An RSR larger than 0 indicates a brain response that is specific to the stimulus rate. Spectral
155 measures such as ITC can be biased by other neural activity than endogenous oscillations: For example,
156 a response caused by the omission of an expected stimulus might produce an increase in ITC that is most
157 pronounced at low frequencies (~250 ms in Fig. 1E). By contrasting ITC between two rate conditions,
158 RSR removes such contamination if it is independent of stimulus rate (i.e. present in both rate

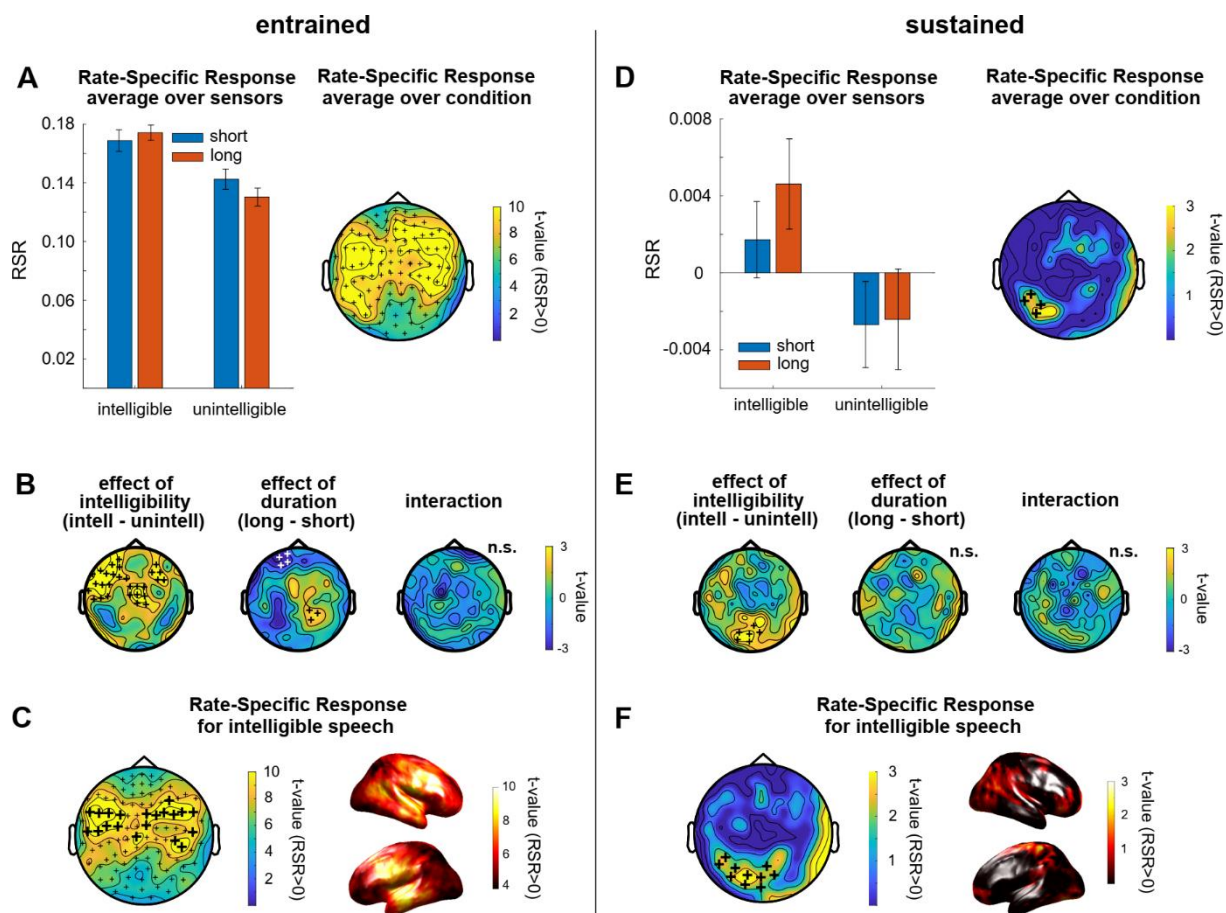
159 conditions). This property makes it – in the present case – also superior to other commonly used
160 approaches, such as permutation tests [21,22], which would not only abolish the hypothesized rhythmic
161 responses, but also non-rhythmic responses which produce high ITC for other reasons (e.g., evoked
162 response to stimulus omission).

163
164 We next defined two time windows of interest (white in Fig. 1E). The first time window (“entrained”)
165 covered the period in which sound sequences were presented while but avoiding sequence onset and
166 offset. This period allows us to measure entrained responses (i.e. neural responses synchronised with an
167 ongoing stimulus). A large RSR in this time window reflects a brain response aligned to the stimulus
168 rhythm (irrespective of whether a true oscillation is involved). The other time window (“sustained”)
169 covered the silent interval between sequences while avoiding sequence offset. A large RSR in this time
170 window is evidence for a sustained oscillatory response and, consequently, for the involvement of
171 endogenous neural oscillations in generating stimulus-aligned entrained responses.

172
173 In the entrained time window, when averaged across all conditions, the RSR was clearly larger than 0
174 (cluster-based correction, $p < 0.001$; summed $t = 883.39$; 102 sensors in cluster), showing a typical
175 auditory scalp topography (Fig. 2A). We then contrasted the RSR across conditions (Fig. 2B). We found
176 a main effect of intelligibility (cluster-based correction, $p < 0.001$; summed $t = 87.30$; total of 29 sensors
177 in 2 clusters), revealing stronger rate-specific responses to intelligible speech in a cluster of left frontal
178 sensors. We also found a main effect of duration, revealing a preference for shorter sequences for left
179 frontal sensors (cluster-based correction, $p = 0.02$; summed $t = -11.11$; 4 sensors in cluster) and one for
180 longer sequences for parietal sensors (cluster-based correction, $p = 0.05$; summed $t = 6.83$; 3 sensors in
181 cluster). There was no significant interaction between intelligibility and duration.

182 Although the RSR was larger for intelligible speech, it was significantly larger than 0 (indicating the
183 presence of an entrained response) for both intelligible (cluster-based correction, $p < 0.001$; summed t
184 $= 783.56$; 102 sensors in cluster) and unintelligible speech (cluster-based correction, $p < 0.001$; summed
185 $t = 706.67$; 102 sensors in cluster). Despite being reliable at all MEG sensors, the effect was localized
186 to superior temporal regions and frontal regions bilaterally (Fig. 2C).

187



188
 189 **Figure 2. Main results from Experiment 1. A-C. Results in the entrained time window. Bars in panel A show RSR in**
 190 **the different conditions, averaged across gradiometers and participants. Error bars show SEM, corrected for within-**
 191 **subject comparison. The topography shows t-values for the comparison with 0, separately for the 102 gradiometer pairs,**
 192 **and after RSR was averaged across conditions. Topographies in B contrast RSR across conditions. Topography and**
 193 **source plots in C show t-values for the comparison with 0 in the intelligible conditions. In all topographic plots, plus**
 194 **signs indicate the spatial extent of significant clusters from cluster-based permutation tests (see Materials and Methods).**
 195 **In B, white plus signs indicate a cluster with negative polarity (i.e. negative t-values) for the respective contrast. In A**
 196 **and C, this cluster includes all gradiometers (small plus signs). In C, larger plus signs show the 20 sensors with the**
 197 **highest RSR, selected for subsequent analyses (Fig. 3). D-F. Same as A-C, but for the sustained time window. Please**
 198 **refer to Data S1 for the numerical values underlying this figure.**

199 In the sustained time window, when averaged across all conditions, the RSR was larger than 0 (cluster-
 200 based correction, $p = 0.05$; summed $t = 9.22$; 4 sensors in cluster) and maximal at left-lateralized parietal
 201 sensors (Fig. 2D). When contrasting RSR across conditions (Fig. 2E), we again found a main effect of
 202 intelligibility (cluster-based correction, $p = 0.01$; summed $t = 15.84$; 6 sensors in cluster), revealing
 203 stronger sustained rate-specific responses for intelligible speech. Importantly, these sustained responses
 204 were only significant (i.e. $RSR > 0$) after intelligible speech (cluster-based correction, $p = 0.01$; summed
 205 $t = 23.00$; 10 sensors in cluster); no significant cluster was found after unintelligible speech. Sustained

206 effects after intelligible speech were localized to fronto-parietal brain regions, with a peak in left parietal
207 regions (Fig. 2F).

208

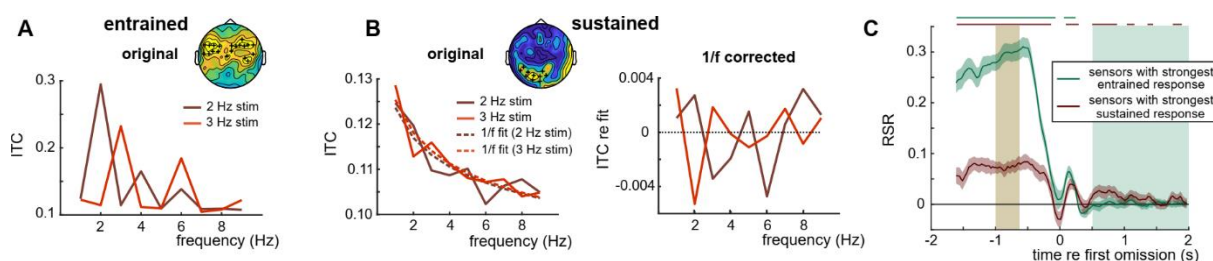
209 To ensure that sustained oscillatory activity was not a result of aperiodic (“1/f”) activity [23], which
210 might differ between the two stimulus rates, we subtracted the “1/f component” from ITC measures of
211 the sustained response (cf. [24]) by applying linear regression with reciprocal frequency (1/f) as a
212 predictor of neural responses. We did this separately for the two stimulus rates, and re-computed the
213 RSR using the residual (see Materials and Methods). This analysis confirms a sustained oscillatory
214 response only after intelligible speech (Fig. S1). Together, these effects demonstrate rhythmic brain
215 responses at a frequency corresponding to the rate of stimulation, which outlast the stimulation at parietal
216 sensors, and are present after intelligible, but not unintelligible rhythmic speech.

217

218 All sensors and conditions were included in our main analyses (Fig. 2). We then explored the observed
219 effects further (Fig. 3), restricting analyses of orthogonal contrasts to sensors which are most important
220 for those main results. For the entrained time window, we selected the 20 sensors with the largest RSR
221 during intelligible speech (large plus signs in Fig. 2C; the significant cluster included all sensors). For
222 the sustained time window, we selected all 10 sensors in the significant cluster obtained after intelligible
223 speech in (Fig. 2F).

224 We first verified that the rate-specific responses, revealed in our main analyses, were produced by
225 responses at both of the stimulus rates tested. We found this to be the case in both entrained (Fig. 3A)
226 and sustained (Fig. 3B) time windows: ITC at both 2 Hz and 3 Hz was significantly higher when it
227 corresponded to the stimulation rate than when it did not (entrained: 2 Hz, $t(20) = 13.11$, $p < 0.0001$; 3
228 Hz, $t(20) = 11.46$, $p < 0.0001$; sustained: 2 Hz, $t(20) = 1.91$, $p = 0.035$; 3 Hz, $t(20) = 2.17$, $p = 0.02$). In
229 the sustained time window, subtracting 1/f components (dashed lines in Fig. 3B) from the data
230 (continuous lines) revealed clearer peaks that correspond to the stimulation rate (or its harmonics). We
231 note again the RSR discards such 1/f components by contrasting ITC values at the same two frequencies
232 across the two stimulus rates.

233 We then tested how rhythmic responses developed over time. Both selected sensor groups (based on
 234 entrained and sustained responses) showed a significant RSR throughout the entrained time window
 235 (horizontal lines in Fig. 3C; FDR-corrected). Importantly, the RSR at sensors selected to show a
 236 sustained response fluctuated at around the time of the first omitted word and then remained significantly
 237 above 0 during intelligible speech for most of the sustained time window. Although the presence of a
 238 sustained RSR is expected (given the method used to select the sensors), this result gives us valuable
 239 insight into the timing of the observed effect. In particular, it excludes the possibility that the sustained
 240 effect is a short-lived consequence of the omission of an expected stimulus (see Discussion).



241
 242 **Figure 3. Follow-up analyses from Experiment 1, using selected sensors (plus signs in insets, reproducing Fig. 2C and**
 243 **F, respectively). A-B. ITC as a function of neural frequency, measured during (A) and after (B) intelligible speech,**
 244 **presented at 2 and 3 Hz. Note that these ITC values were combined to form RSR shown in Fig. 2, as described in Fig.**
 245 **1F. For the right panel in B, a fitted “1/f” curve (shown as dashed lines in the left panel) has been subtracted from the**
 246 **data (see Materials and Methods). Note that the peaks correspond closely to the respective stimulus rates, or their**
 247 **harmonics (potentially produced by imperfect sinusoidal signals). C. RSR during intelligible speech as a function of**
 248 **time, for the average of selected sensors. Horizontal lines on top of the panel indicate an FDR-corrected p-value of \leq**
 249 **0.05 (t-test against 0) for the respective time point and sensor group. Shaded areas correspond to the two defined time**
 250 **windows (brown: entrained, green: sustained). Shaded areas around the curves show SEM. Please refer to Data S1**
 251 **for the numerical values underlying this figure.**

252
 253 We did not measure the success of speech perception in Experiment 1. This is because such a task would
 254 have biased participants to attend differently to stimuli in intelligible conditions, making comparisons
 255 with neural responses in our unintelligible control condition difficult. Similarly, we refrained from using
 256 tasks which might have biased our measurement of endogenous oscillations in the silent period. For
 257 example, tasks in which participants are asked to explicitly predict an upcoming stimulus might have
 258 encouraged them to imagine or tap along with the rhythm. Our irregularity detection task was therefore
 259 primarily designed to ensure that participants remain alert and focused and not to provide behavioural
 260 relevance of our hypothesized sustained neural effect. Nevertheless, we correlated the RSR in both time

261 windows (and at the selected sensors) with performance in the irregularity detection task (Fig. S2). We
 262 found a significant correlation between RSR in the entrained time window and detection performance
 263 (Pearson's $r = 0.53$, $p = 0.01$), demonstrating behavioural relevance of entrained brain responses.
 264 Perhaps unsurprisingly, given that there is no temporal overlap between the sustained response and
 265 target presentation, individual differences in the sustained RSR did not show a significant correlation
 266 with individual differences in rhythm perception ($r = 0.27$, $p = 0.28$).

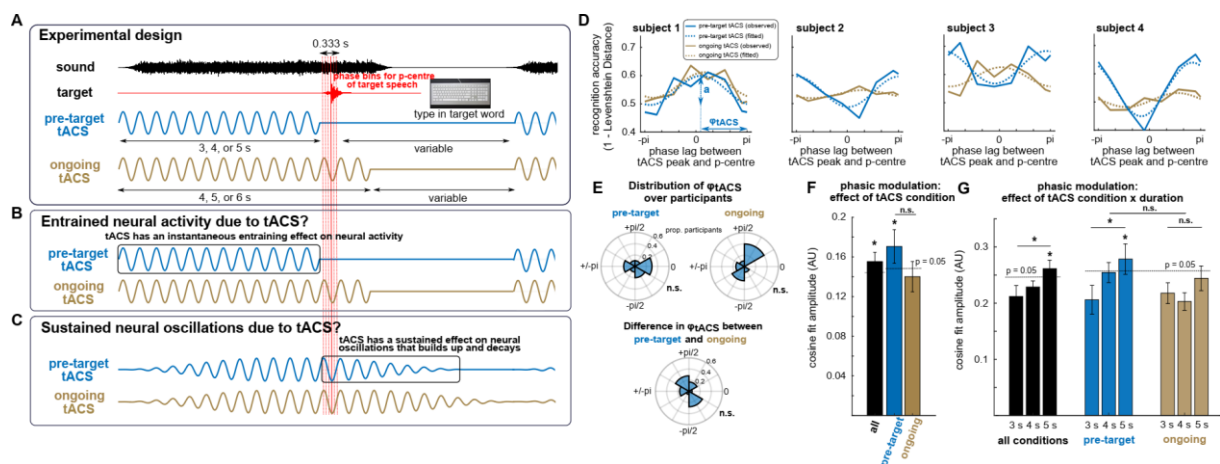
267

268 *Experiment 2: tACS produces sustained rhythmic fluctuations in word report accuracy*

269 In Experiment 1, we showed sustained oscillatory activity after rhythmic sequences of intelligible
 270 speech, indicating that endogenous neural oscillations are involved in generating speech-entrained brain
 271 responses. In Experiment 2, we tested whether tACS produces sustained rhythmic changes in speech
 272 perception; if observed this would not only provide an equivalent demonstration for tACS (i.e. that
 273 endogenous neural oscillations are entrained by transcranial electrical stimulation), but also show that
 274 these endogenous neural oscillations causally modulate perceptual outcomes.

275

276 Twenty participants were asked to report a single spoken, 16-channel vocoded target word, recorded
 277 rhythmically at 3 Hz, and embedded in background noise (Fig. 4A). The signal-noise ratio between
 278 target word and noise was adjusted for individual participants, ensuring similar task difficulty across
 279 participants and ensuring that effects of tACS were not obscured by floor or ceiling report accuracy (see
 280 Materials and Methods).



281

282 **Figure 4. Experimental paradigm and main results from Experiment 2. A. Experimental paradigm. In each trial, a**
283 **target word (red), embedded in noise (black), was presented so that its p-centre falls at one of six different phase lags**
284 **(vertical red lines; the thicker red line corresponds to the p-centre of the example target), relative to preceding (“pre-**
285 **target tACS”) or ongoing tACS (which was then turned off). After each trial, participants were asked to type in the**
286 **word they had heard. The inset shows the electrode configuration used for tACS in both conditions. B,C. Theoretical**
287 **predictions. B. In the case of entrained neural activity due to tACS, this would closely follow the applied current and**
288 **hence modulate perception of the target word only in the ongoing tACS condition. C. In the case that true oscillations**
289 **are entrained by tACS, these would gradually decay after tACS offset and a “rhythmic entrainment echo” might**
290 **therefore be apparent as a sustained oscillatory effect on perception even in the pre-target condition. D. Accuracy in**
291 **the word report task as a function of phase lag (relative to tACS peak shown in A), averaged across tACS durations,**
292 **and for four example participants. Phasic modulation of word report was quantified by fitting a cosine function to data**
293 **from individual participants (dashed lines). The amplitude (a) of this cosine reflects the magnitude of the hypothesized**
294 **phasic modulation. The phase of this cosine (φ_{tACS}) reflects the distance between its peak and the maximal phase lag of**
295 **π . Note that the phase lag with highest accuracy for the individual participants, estimated based on the cosine fit,**
296 **therefore corresponds to $\pi - \varphi_{tACS}$. E. Distribution of φ_{tACS} in the two tACS conditions, and their difference. F,G.**
297 **Amplitudes of the fitted cosines (cf. amplitude a in panel D), averaged across participants. In F, cosine functions were**
298 **fitted to data averaged over tACS duration (cf. panel D). In G, cosine functions were fitted separately for the three**
299 **durations. For the black bars, cosine amplitudes were averaged across the two tACS conditions. Dashed lines show the**
300 **threshold for statistical significance ($p \leq 0.05$) for a phasic modulation of task accuracy, obtained from a surrogate**
301 **distribution (see Materials and Methods). Error bars show SEM (corrected for within-subject comparisons in F). Please**
302 **refer to Data S1 for the numerical values underlying panels E-G.**
303

304 While participants performed this task, tACS was applied at 3 Hz over auditory regions, using the same
305 configuration of bilateral circular and ring electrodes that yielded successful modulation of speech
306 perception in [8] (see inset of Fig. 4A). In each trial, the target word was presented so that its “perceptual
307 centre” (see Materials and Methods) falls at one of six different phase lags (red lines in Fig. 4A), relative
308 to tACS. Prior to target presentation, tACS was applied for ~3, 4, or 5 seconds. Importantly, the target
309 word was presented either during tACS (“ongoing tACS”), which was turned off shortly afterwards, or
310 immediately after tACS (“pre-target tACS”). We hypothesized that entrained neural activity due to tACS
311 (irrespective of whether it involves endogenous oscillations; Fig. 4B) will produce a phasic modulation
312 of speech perception in the ongoing tACS condition, as reported previously [8–10]. However, in the pre-
313 target tACS condition, such a phasic modulation can only be explained by sustained neural oscillations
314 which lead to rhythmic changes in perception (Fig. 4C).

315

316 Accuracy in reporting the target word was quantified using Levenshtein distance (similar to the
317 proportion of phonemes reported correctly [25]; see Materials and Methods). When averaged across

318 phase lags, word report accuracy was slightly higher in the pre-target tACS condition (0.50 ± 0.09 , mean
319 \pm std) than in the ongoing tACS condition (0.49 ± 0.09), but not significantly different ($t(19) = 1.67$, p
320 $= 0.11$; repeated-measures t-test). This result indicates that the two tACS conditions did not reliably
321 differ in their generic (i.e. phase-independent) effects on speech perception.

322

323 For each participant, and separately for the two tACS conditions, we determined how task accuracy
324 varies with tACS phase lag (Fig. 4D). We then fitted a cosine function to data from individual
325 participants (dashed lines in Fig. 4D). The amplitude of the cosine reflects how strongly speech
326 perception is modulated by tACS phase. The phase of the cosine, labeled φ_{tACS} , reflects the distance
327 between the peak of the cosine and the maximal phase lag tested (defined as π ; Fig. 4D). For example,
328 a φ_{tACS} of π would indicate highest word report accuracy at a tACS phase lag of 0.

329

330 Previous studies have reported that “preferred” tACS phase (leading to highest accuracy) varies across
331 participants [7–10]. Indeed, in neither of the two conditions did we find evidence for a non-uniform
332 distribution of φ_{tACS} (Fig. 4E) across participants (Rayleigh’s test for non-uniformity; pre-target tACS:
333 $z(19) = 0.64$, $p = 0.53$; ongoing tACS: $z(19) = 0.71$, $p = 0.50$). We also failed to reveal a non-uniform
334 distribution of the individual phase differences between conditions ($\varphi_{tACS(ongoing)} - \varphi_{tACS(pre-target)}$;
335 $z(19) = 0.24$, $p = 0.79$), indicating that the perceptual outcome in the ongoing and pre-target tACS
336 conditions might not rely on identical neural processes.

337

338 To statistically evaluate the hypothesized phasic modulation of word report accuracy, we compared the
339 observed cosine amplitudes (Fig. 4F,G) with a surrogate distribution – an approach which has recently
340 been shown to be highly sensitive to detect such a phasic effect [21]. The surrogate distribution was
341 obtained by repeatedly shuffling experimental variables assigned to individual trials and extracting
342 cosine amplitudes for each of those permutations. Here, these variables can refer to tACS phase lags,
343 conditions, or durations, depending on the comparison of interest (see Materials and Methods).

344

345 We first pooled data over tACS durations (3, 4, and 5 s) before extracting cosine amplitudes (Fig. 4F).
346 When tACS conditions were combined (i.e. their cosine amplitudes averaged), we found a significant
347 phasic modulation of word report accuracy ($z(19) = 2.80, p = 0.003$). When conditions were analyzed
348 separately, we found a significant phasic modulation of word report accuracy in the pre-target tACS
349 condition ($z(19) = 2.96, p = 0.002$). This effect was not statistically reliable in the ongoing tACS
350 condition ($z(19) = 0.98, p = 0.16$). However, the difference in modulation strength between tACS
351 conditions was not significantly different from that obtained in a surrogate distribution ($z(19) = 1.37, p$
352 $= 0.17$), indicating that the two conditions did not reliably differ in their efficacy of modulating speech
353 perception.

354 We next tested whether the phasic modulation of speech perception depends on tACS duration (Fig.
355 4G). When tACS conditions were combined, we found an increase in phasic modulation of word report
356 accuracy from 3-s tACS to 5-s tACS that was significantly larger than that observed in a surrogate
357 distribution ($z(19) = 1.82, p = 0.03$). After five seconds of tACS, the phasic modulation was significant
358 ($z(19) = 2.36, p = 0.01$), while the modulation was not statistically reliable after three seconds of
359 stimulation ($z(19) = -0.52, p = 0.70$). When tACS conditions were analyzed separately, a significant
360 effect of duration was observed in the pre-target tACS condition ($z(19) = 1.86, p = 0.03$), but not in the
361 ongoing tACS condition ($z(19) = 0.69, p = 0.24$). After five seconds of tACS, the phasic modulation of
362 word report accuracy was significant in the pre-target tACS condition ($z(19) = 2.15, p = 0.016$), but not
363 in the ongoing tACS condition ($z(19) = 1.17, p = 0.12$). However, when effects of duration (3-s tACS
364 vs 5-s tACS) were compared across tACS conditions, we did not find a reliable difference between the
365 two ($z(19) = 0.90, p = 0.37$), indicating that there was no significant interaction between tACS condition
366 and duration.

367

368 Together, we found rhythmic changes in speech perception after the offset of tACS, which depend on
369 the duration of the preceding stimulation. This finding demonstrates that tACS can induce rhythmic
370 changes in neural activity that build up over time and continue beyond the period of stimulation. Both
371 of these effects are consistent with endogenous neural oscillations being entrained by tACS.

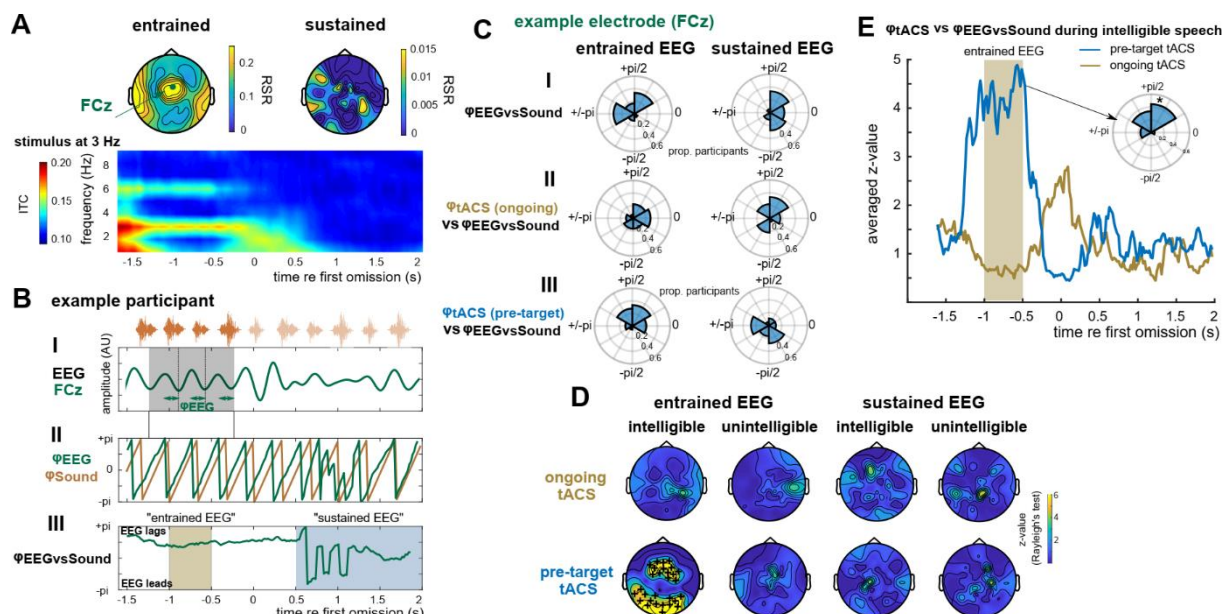
372

373 *Experiment 1 vs 2: Phase of speech-entrained EEG predicts tACS effects in single participants*

374 In line with previous research [7–10], we found that participants differ in the tACS phase leading to
 375 more or less accurate perception, reflected by φ_{tACS} (Fig. 4E). Although adapting tACS protocols to
 376 individual participants has been suggested as a crucial step to increase effect sizes and advance the field
 377 [26–28], neural parameters that can predict these individual differences remain elusive. Here, we report
 378 an analysis of combined data from 18 participants who participated in both our experiments. Rather than
 379 the MEG data reported earlier, we analysed the concurrent EEG data collected during Experiment 1 and
 380 relate this to tACS effects observed in Experiment 2 in the same participants. This is because EEG is
 381 methodologically closer related to tACS than MEG: Both tACS and EEG, but not MEG, are similarly
 382 affected by distortions in current flow in the skull and other, non-neural tissues [29–32]. We therefore
 383 tested whether we can use EEG data to predict individual differences in φ_{tACS} .

384

385 In line with the MEG results reported earlier, EEG data in Experiment 1 showed a highly reliable rate-
 386 specific response (RSR) in the entrained time window (Fig. 5A; $p < 0.001$; cluster-based correction).
 387 The RSR in the sustained time window was largest at fronto-parietal electrodes, similar to our reported
 388 findings in MEG. However, this sustained effect was not statistically reliable (i.e. no significant clusters
 389 were obtained). This could either be due to the lower signal-to-noise ratio of EEG or because EEG and
 390 MEG measure non-identical neural sources [33], which makes it possible that only one of the two
 391 methods captures a neural process of interest.



392

393 **Figure 5. Combining Experiments 1 and 2. A. EEG results from Experiment 1. Topographies show RSR in the**
394 **intelligible conditions. The time-frequency representation depicts ITC during 3-Hz sequences, averaged across EEG**
395 **electrodes, participants, and conditions (cf. Fig. 1C). B. Illustration of methodological approach, using example data**
396 **from one participant and electrode (FCz, green in panel A). B-I. Band-pass filtered (2-4 Hz) version of the EEG signal**
397 **that has been used to estimate φ_{EEG} in the panel below (B-II). In practice, EEG phase at 3 Hz was estimated using FFT**
398 **applied to unfiltered EEG data. Consequently, φ_{EEG} reflects the distance between the peaks of a cosine, fitted to data**
399 **within the analysis window (shaded grey), and the end of each 3-Hz cycle (green arrows). B-II. φ_{EEG} (green; in the**
400 **intelligible conditions and averaged across durations) and phase of the 3-Hz sequence (φ_{Sound} , orange). The latter is**
401 **defined so that the perceptual centre of each word corresponds to phase π (see example sound sequence, and its**
402 **theoretical continuation, on top of panel B-I). B-III. Circular difference between φ_{EEG} (green in B-II) and φ_{Sound}**
403 **(orange in B-II), yielding $\varphi_{EEGvsSound}$. Given that φ is defined based on a cosine, a positive difference means that EEG**
404 **lags sound. C. Distribution of individual $\varphi_{EEGvsSound}$, and its relation to φ_{tACS} . Data from one example electrode (FCz)**
405 **is used to illustrate the procedure; main results and statistical outcomes are shown in panel D. C-I. Distribution of**
406 **$\varphi_{EEGvsSound}$ (cf. B-III), extracted in the intelligible conditions, and averaged across durations and within the respective**
407 **time windows (shaded brown and blue in B-III, respectively). C-II,III: Distribution of the circular difference between**
408 **φ_{tACS} (Fig. 4E) and $\varphi_{EEGvsSound}$ (C-I). Note that a non-uniform distribution (tested in panel D) indicates a consistent**
409 **lag between individual φ_{tACS} and $\varphi_{EEGvsSound}$. D. Z-values (obtained by means of a Rayleigh's test; see Materials and**
410 **Methods), quantifying non-uniformity of the distributions shown in C-II,III for different combinations of experimental**
411 **conditions. Plus signs show electrodes selected for follow-up analyses (FDR-corrected $p \leq 0.05$). E. Z-values shown in**
412 **D for intelligible conditions as a function of time, averaged across selected EEG sensors (plus signs in D). For the**
413 **electrode with the highest predictive value for tACS (F3), the inset shows the distribution of the circular difference**
414 **between φ_{tACS} and $\varphi_{EEGvsSound}$ in the pre-target condition, averaged within the entrained time window (shaded**
415 **brown). Please refer to Data S1 for the numerical values underlying panels A,C-E.**

416

417 Although the RSR combines ITC measured during two different stimulus rates (Fig. 1E,F), we here
418 focused on EEG responses at 3 Hz in response to 3-Hz sequences, corresponding to the frequency of
419 tACS in Experiment 2. Fig. 5B,C illustrates our analysis procedure for one example participant (Fig.
420 5B) and EEG electrode (Fig. 5B,C). For each EEG electrode, we extracted the phase of the 3-Hz
421 response at each time point throughout the trial, and labeled it φ_{EEG} (Fig. 5B-II, green). We used Fast
422 Fourier Transformation (FFT) to estimate φ_{EEG} (see Materials and Methods), which is equivalent to
423 fitting a cosine at the frequency of interest (i.e. 3 Hz) to data in the analysis window (shaded grey in Fig.
424 5B-I) and extracting its phase. The value of φ_{EEG} therefore corresponds to the distance between each of
425 the three peaks of the fitted cosine and the end of the corresponding cycle (defined as π ; Fig. 5B-I)

426

427 For each participant and EEG electrode, we determined how φ_{EEG} relates to the timing of the presented
428 sound sequences (φ_{Sound} ; Fig. 5B-II, blue). Assuming rhythmic EEG responses reliably following the

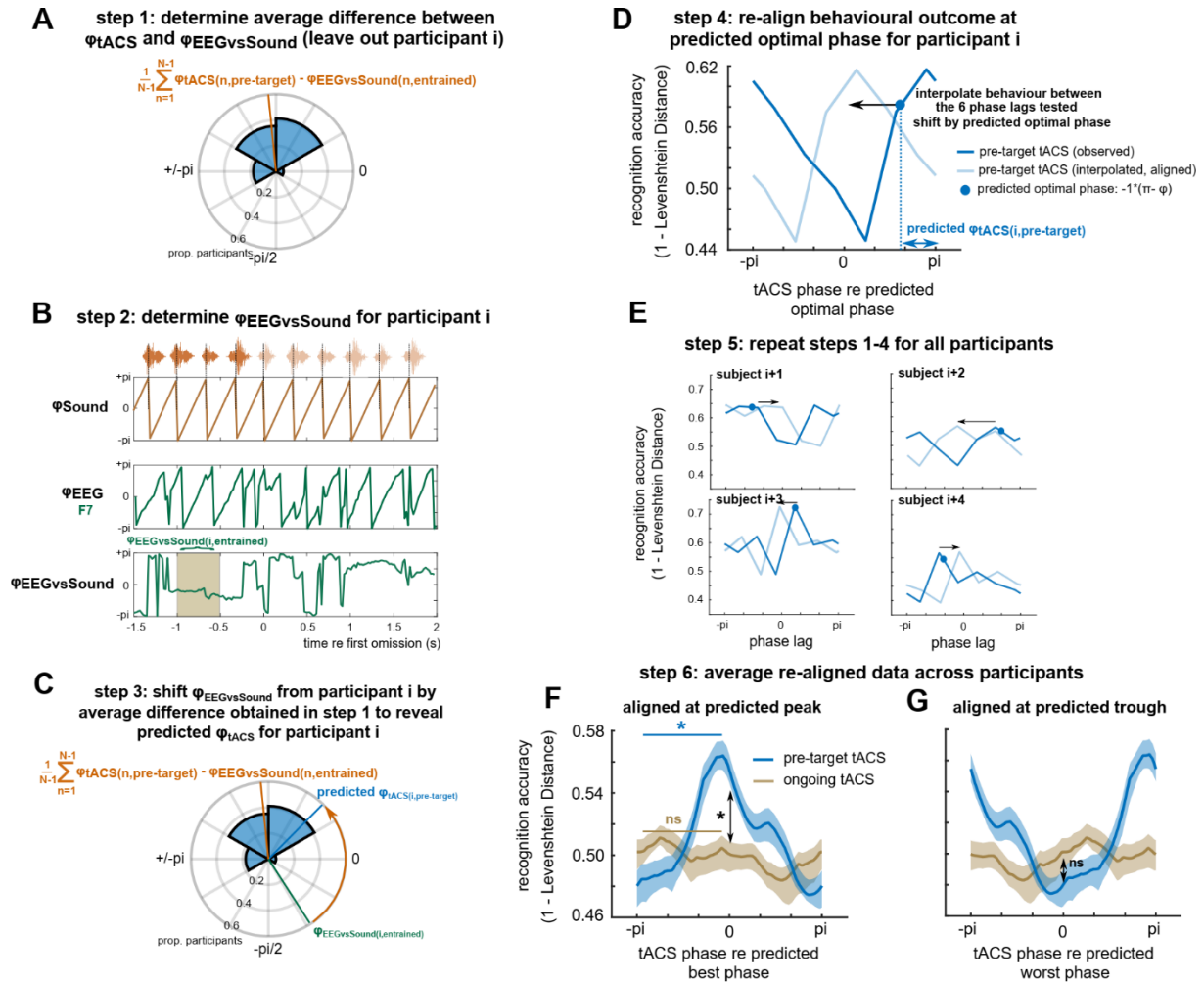
429 presented sequences, the phase relation between EEG and sound (i.e. their circular difference) should
430 be approximately constant over time. This phase relation, labeled $\varphi_{EEGvsSound}$ (Fig. 5B-III), was
431 therefore averaged within each of the two time windows of interest (entrained and sustained). The
432 distribution of $\varphi_{EEGvsSound}$ across participants in these time windows is shown in Fig. 5C-I for the
433 selected EEG electrode.

434 For each participant, EEG electrode, and the two time windows, we then calculated the (circular)
435 difference between $\varphi_{EEGvsSound}$ and φ_{tACS} in the ongoing (Fig. 5C-II) and pre-target tACS conditions
436 (Fig. 5C-III), respectively. Importantly, a non-uniform distribution would indicate a consistent lag
437 between φ_{tACS} and $\varphi_{EEGvsSound}$ across participants. Fig. 5D shows the degree of non-uniformity of
438 these distributions (as the z-values obtained in Rayleigh's test for non-uniformity; see Materials and
439 Methods), for all EEG electrodes, and different combinations of conditions in the two experiments. We
440 found that the phase relation between EEG and intelligible speech in the entrained time window
441 significantly predicts φ_{tACS} in the pre-target tACS condition. This effect was maximal at fronto-central
442 EEG electrodes (e.g., F3: $z(17) = 8.88$, $p = 0.003$, FDR-corrected for 70 electrodes). While main results
443 are shown for all electrodes and conditions (Fig. 5D), we again restricted follow-up analyses to those
444 which are most relevant, and based on orthogonal contrasts. Here, we found that $\varphi_{EEGvsSound}$ was most
445 predictive for φ_{tACS} around the presentation of the last word in the sequence (Fig. 5E). At the sensor
446 with the strongest effect (F3), we observed a shift of ~ 90 degrees (corresponding to ~ 83.3 ms) between
447 φ_{tACS} and $\varphi_{EEGvsSound}$ (inset in Fig. 5E). As expected from its increased dissimilarity to tACS, MEG
448 responses measured in Experiment 1 did not reveal any predictive value for tACS results from
449 Experiment 2 (Fig. S3).

450

451 Findings shown in Fig. 5 have important implications for future studies: Given the previous reports of
452 tACS-induced changes in speech processing [7–11], tACS may be a promising tool to treat conditions
453 associated with deficits in speech comprehension. However, individual differences in φ_{tACS} have so far
454 hampered this goal – existing data suggest that different tACS phases will lead to optimal perception for
455 each individual participant and extensive testing might therefore be needed to determine this optimal
456 phase before further interventions. Based on the consistent phase shift between $\varphi_{EEGvsSound}$ and φ_{tACS}

457 shown in Figure 5E, however, it should be possible to predict optimal tACS phase for single participants
458 from EEG responses aligned to rhythmic intelligible speech. We tested this prediction in an additional
459 analysis, as illustrated in Fig. 6 (see also Materials and Methods). This analysis was designed to illustrate
460 the implications of findings depicted in Fig. 5D for future applications (e.g., when optimising tACS
461 methods for use in interventions), rather than for providing new results. We selected EEG data from the
462 entrained time window and the EEG electrode (F3) which was most predictive for effects of pre-target
463 tACS (Fig. 5D), and behavioural data from the same tACS condition. Such a selection is permitted as
464 main results were already reported – without pre-selection – in Fig. 5D. For each participant i , we
465 determined their individual $\varphi_{EEGvsSound}$ (Fig. 6B) and used it to estimate their individual φ_{tACS} (Fig.
466 6C), based on the difference between the two that was observed on the group level (Fig. 6A,C).
467 Importantly, for the latter, data from participant i was excluded, avoiding circularity of the procedure.
468 For each participant, the estimated φ_{tACS} was then used to predict the tACS phase lag with highest
469 accuracy in the word report task (blue dot in Fig. 6D,E). The behavioural data collected in Experiment
470 2 was re-aligned, relative to this predicted optimal phase lag (Fig. 6D; see Fig. S4 for individual re-
471 aligned data from all participants). The outcome, averaged across participants, is shown in Fig. 6F (blue).
472 As intended, word report accuracy was highest at the predicted optimal phase lag (0 in Fig. 6F), and
473 significantly higher than in the opposite phase bin ($\pm\pi$ in Fig. 6F), which should lead to worst
474 performance ($t(17) = 4.49$, $p < 0.001$). This result confirms that optimal tACS phases for speech
475 perception can be estimated, exclusively based on individual EEG data (if the average difference
476 between φ_{tACS} and $\varphi_{EEGvsSound}$ is known).



477

478 **Figure 6. Predicted individual preferred tACS phases in the pre-target tACS condition from EEG data measured in the**
 479 **entrained time window at sensor F3. A, Step 1: For each participant i , data from all remaining participants was used to**
 480 **estimate the average difference between ϕ_{tACS} and $\phi_{EEGvsSound}$. B, Step 2: $\phi_{EEGvsSound}$ was determined for participant**
 481 **i . C, Step 3: This $\phi_{EEGvsSound}$ was shifted by the phase difference obtained in step 1, yielding the predicted ϕ_{tACS} for**
 482 **participant i . D, Step 4: The predicted ϕ_{tACS} was used to estimate the tACS phase lag with highest perceptual accuracy**
 483 **for participant i , and the corresponding behavioural data was shifted so that highest accuracy was located at a centre**
 484 **phase bin. Prior to this step, the behavioural data measured at the six different phase lags was interpolated to enable**
 485 **re-alignment with higher precision. E, Step 5: This procedure was repeated for all participants. F, Step 6: The re-aligned**
 486 **data was averaged across participants (blue). For comparison, the procedure was repeated for the ongoing tACS**
 487 **condition (using EEG data from the same sensor; brown). The shaded areas show SEM, corrected for within-subject**
 488 **comparison. G. Same as in F, but aligned at the predicted worst phase for word report accuracy. Please refer to Data**
 489 **S1 for the numerical values underlying panels F and G.**

490

491 *Sustained oscillations produced by tACS enhance, but do not disrupt speech perception*

492 It remains debated whether a phasic modulation of speech perception, produced by tACS, reflects an
 493 enhancement or disruption of perception, or both [8–11,34]. Given that $\phi_{EEGvsSound}$ was not predictive
 494 of ϕ_{tACS} in the ongoing tACS condition (Fig. 5D), we used data from the latter to test this question. We

495 used the procedure illustrated in Fig. 6 (using data from the same EEG sensor F3) to predict optimal
496 tACS phases in the ongoing tACS condition (see Materials and Methods). As $\varphi_{EEGvsSound}$ does not
497 predict φ_{tACS} in this condition, any tACS-dependent modulation of task accuracy should be abolished
498 by the re-alignment, and the re-aligned data (Fig. 6F, brown) should therefore reflect the null hypothesis,
499 i.e. task outcome in the absence of a phasic modulation. Indeed, word report accuracy was not higher at
500 the predicted optimal phase lag for the ongoing tACS condition than at the opposite phase lag ($t(17) =$
501 $0.08, p = 0.53$).

502 Given that entrained EEG is predictive for φ_{tACS} only in the pre-target tACS condition (Fig. 5D), there
503 must be some phase bins in which accuracy differs between the two tACS conditions after EEG-based
504 re-alignment. However, these previous analyses did not reveal the *direction* of this difference
505 (enhancement vs disruption). We therefore compared performance at the predicted optimal tACS phase
506 between the two tACS conditions and found higher word report accuracy in the pre-target tACS
507 condition ($t(17) = 3.48, p = 0.001$). For both conditions, we then re-aligned the behavioural data again,
508 but this time at the tACS predicted to be worst for performance (i.e. 180° away from the tACS phase
509 predicted to be optimal for performance). Performance at the predicted worst tACS phase did not
510 significantly differ between the two conditions ($t(17) = 1.34, p = 0.90$). These results show that the
511 sustained phasic modulation of word report accuracy, produced by pre-target tACS, reflects an
512 enhancement of speech perception both relative to a non-optimal tACS phase and compared to EEG-
513 aligned data from an ongoing tACS condition in which EEG data was not predictive of optimal tACS
514 phase.

515

516 **Discussion**

517 In 1949, Walter & Walter [35] observed that rhythmic sensory stimulation produces rhythmic brain
518 responses. Importantly, in their paper, when listing potential explanations for their observation, they
519 distinguished “fusion of evoked responses giving an accidental appearance of rhythmicity” from “true
520 augmentation or driving of local rhythms at the frequency of the stimulus”. Now, more than 70 years
521 later, it remains an ongoing debate whether “neural entrainment”, brain responses aligned to rhythmic
522 input, is due to the operation of endogenous neural oscillations or reflects a regular repetition of

523 stimulus-evoked responses [16,36–39]. In two experiments, we provide clear evidence for entrained
524 endogenous neural oscillations, by showing that rhythmic brain responses and rhythmic modulation of
525 perceptual outcomes can outlast rhythmic sensory and electrical stimulation. We will discuss the
526 implication of these sustained effects of sensory and electrical stimulation, before considering the
527 functional interpretation of neural after-effects. We finish by discussing the potential for practical
528 application of our combined EEG and tACS findings in supporting impaired speech perception.

529

530 *Endogenous neural oscillations entrained by rhythmic sensory and electrical stimulation*

531 Previous studies in a range of domains have similarly demonstrated sustained oscillatory effects after
532 rhythmic sensory stimulation (summarized in [16]). Both perception and electrophysiological signals
533 have been shown to briefly oscillate after a rhythmic sequence of simple visual [40–42] or auditory [43–
534 45] stimuli, such as flashes or pure tones. A recent study showed that such a sustained rhythmic response
535 occurs when preceded by a stimulus evoking the perception of a regular beat, but not when participants
536 merely expect the occurrence of a rhythmic event [46]. Although neural entrainment is widely explored
537 in speech research [1,2], we are only aware of one study reporting sustained oscillatory effects produced
538 by human speech: Kösem et al [17] showed that, immediately after a change in speech rate, oscillatory
539 MEG responses can still be measured at a frequency corresponding to the preceding speech (summarized
540 in [15]). Our results in Experiment 1 are in line with this study and extend it by showing that (1) sustained
541 oscillations produced by speech can be measured in silence and (2) are not observed for acoustically-
542 matched speech stimuli that are unintelligible. Similar effects of intelligibility on neural entrainment
543 have been described for combined tACS and fMRI: Neural responses in the STG to intelligible speech,
544 but not to unintelligible speech, were modulated by tACS [7]. In Experiment 1, we also replicated our
545 previous MEG finding of more reliable stimulus-aligned responses to intelligible than unintelligible
546 speech [5,6]. We further show that (1) rhythmic responses to intelligible speech persist after the offset
547 of the speech stimulus and (2) this sustained effect is absent for acoustically-matched, unintelligible
548 speech. Our results should not be taken as evidence that endogenous neural oscillations are irrelevant
549 for the processing of sounds other than human speech (e.g., [43–45]). However, they might suggest that
550 endogenous oscillations are optimized to process speech, due to its quasi-rhythmic properties [3,47].

551 Additionally, it is possible that the increased salience of intelligible speech (as compared to noise or
552 tone stimuli) enhances participants' alertness and encourages higher-level processing, which has been
553 shown to lead to enhanced oscillatory tracking of rhythmic structures [48,49]. Together, our MEG
554 findings suggest that endogenous neural oscillations are active during neural entrainment, and that these
555 oscillatory mechanisms are of particular importance for processing intelligible speech.

556

557 It is well established that the omission of an expected stimulus evokes a prominent neural response [50–
558 53]. One concern that could be raised regarding the present findings is whether our sustained effects
559 could have been generated by an omission response rather than true oscillatory activity. Several aspects
560 of our Experiment 1 suggest that omission-evoked responses are unlikely to explain the sustained effects
561 of rhythmic stimulation: (1) omission responses would only lead to a sustained RSR if they were specific
562 to the stimulation rate (i.e. if the omission leads to an increase in 2-Hz ITC after 2-Hz sequences and 3-
563 Hz ITC after 3-Hz sequences); (2) sustained oscillatory activity after the end of a sequence lasts longer
564 than would be expected from a single, punctate omission response (see Fig. 3C); (3) previous
565 observations of omission responses show that these are largely generated in brain regions that were most
566 active while rhythmic stimuli were presented [52,53], whereas our study showed sustained responses in
567 brain regions that were not the primary driver of responses measured during sensory stimulation
568 (compare scalp topographies and source distributions in Fig. 2C and 2F). These findings therefore
569 suggest that sustained activity is generated by true oscillatory neural activity produced in response to
570 intelligible speech.

571

572 Several studies have reported modulation of speech perception outcomes by tACS, and conclude that
573 changes in neural entrainment, produced by varying the phase relation between tACS and speech
574 rhythm, are responsible [8–11]. However, thus far these effects could reflect the rhythmic nature of the
575 applied current, which might interfere with processing of speech presented with the same rhythm
576 without any involvement of neural oscillations [15]. In Experiment 2, we found sustained rhythmic
577 fluctuations in speech perception that continued after the offset of tACS. Our results are an important
578 extension of previous work as they suggest that: (1) modulation of speech perception can be due to the

579 operation of neural oscillations entrained by tACS, and (2) sustained oscillatory effects after tACS can
580 be measured in word report outcomes, and hence are causally relevant for speech perception. These
581 findings for speech have precedent in other sensory modalities and brain regions. For example, a recent
582 study [54] used tACS at 7 Hz to stimulate parietal-occipital regions and reported sustained rhythmic
583 EEG responses at the frequency of electric stimulation. Although the functional role of these sustained
584 neural effects for perceptual processes (such as perceptual integration) remain unclear, this previous
585 study provides evidence for neural oscillations entrained by tACS that parallels the present work. The
586 tACS method used here, in which perceptual effects are observed subsequent to the end of electrical
587 stimulation are clearly amenable to further exploration in studies combining tACS and EEG.

588

589 In Experiment 2, the phasic modulation of speech perception observed *after* tACS (in the pre-target
590 tACS condition) was not significantly different from that *during* tACS (in the ongoing tACS condition).
591 In light of results from Experiment 1, where the sustained rhythmic response was clearly weaker than
592 the entrained one, this might seem surprising. Importantly however, the process that interferes with our
593 ability to measure endogenous oscillations during rhythmic stimulation is not identical in the two
594 experiments. In Experiment 1, rhythmic sensory stimulation produced strong, regular evoked activity
595 which dominates the response in the entrained time window. In Experiment 2, the current applied during
596 tACS alternated regularly between periods of strong stimulation (at the tACS peaks and troughs) and no
597 stimulation (at the zero crossings). This, according to our assumptions, might produce rhythmic
598 modulation of speech perception that does not necessarily involve endogenous oscillations (perception
599 might simply “follow” the amount of current injected). However, tACS is not strong enough to evoke
600 neural activity [55,56], and the described effect will not dominate responses as strongly as sensory
601 stimulation in Experiment 1. Moreover, such a phasic effect on speech perception does not necessarily
602 combine additively with that produced by entrained endogenous oscillations – indeed, these two
603 processes might even interfere with each other. Consequently, and in line with our results, rhythmic
604 modulation of speech perception is not necessarily expected to be stronger when both processes interact
605 (regular changes in current vs entrained oscillations in the ongoing tACS condition) as compared to an
606 effect that is due to endogenous oscillations alone (in the pre-target tACS condition).

607

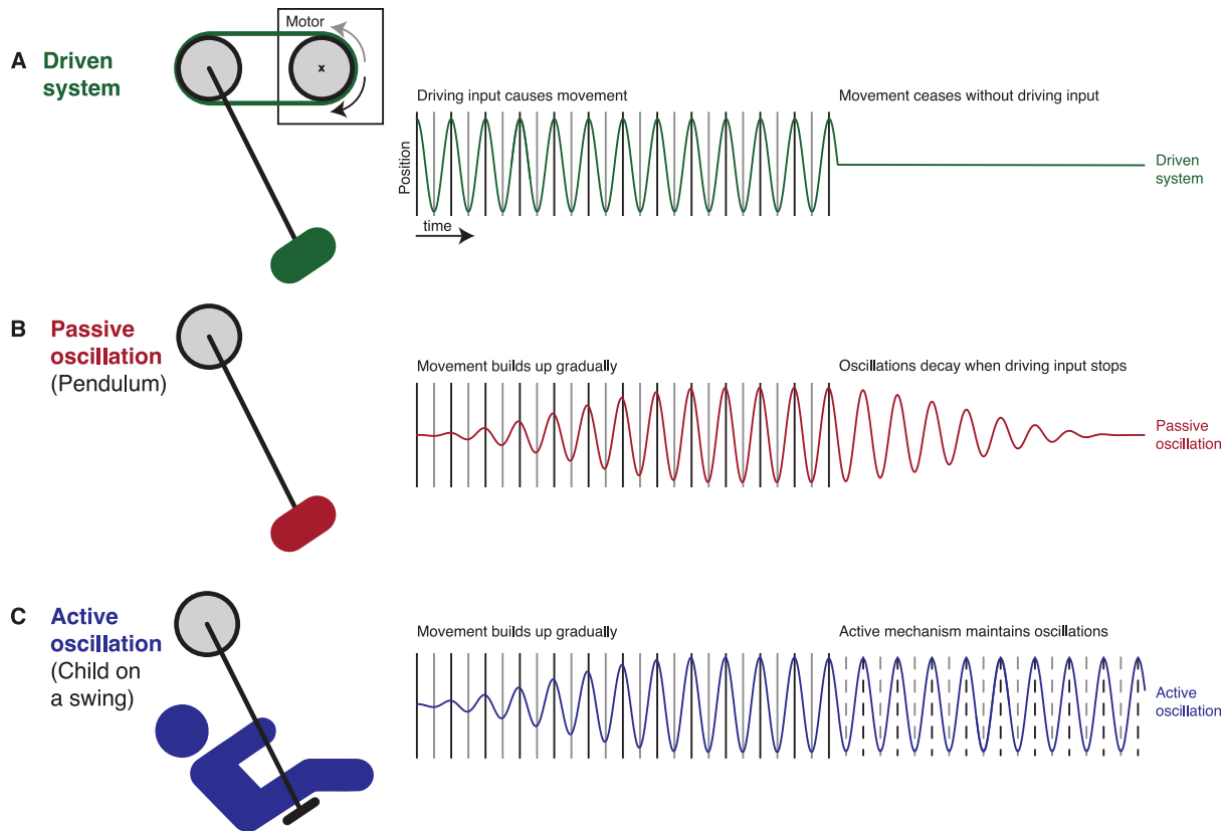
608 Another line of evidence for endogenous oscillations entrained by a rhythmic stimulus comes from
609 studies testing how brain responses vary as a function of stimulus rate and intensity (summarized in
610 [16]). It is a clear prediction from classical physical models that the intensity required to entrain
611 endogenous oscillations decreases when the rate of the entraining stimulus approaches their natural
612 frequency [57–60]. Indeed, this phenomenon, termed “Arnold Tongue”, has recently been observed for
613 visual stimulation [61]. There is tentative evidence that tACS-induced responses behave in a similar way
614 (summarized in [59]), but more studies are needed to substantiate this claim. Based on similar reasoning,
615 entrainment effects should also be stronger when the system has “more time” to align with the external
616 oscillator [59,62]. Our finding that tACS effects on perception increase with stimulation duration (Fig.
617 4G) is therefore clearly in line with oscillatory models. Importantly, such a behaviour was apparent in
618 the pre-target tACS condition, in which effects of endogenous oscillations could be distinguished from
619 those of other, potentially interfering neural processes. Although effects of tACS duration on behaviour
620 were numerically larger and only statistically reliable in this condition, we hesitate to conclude that the
621 effect is specific to pre-target tACS since the condition by duration interaction was not reliable.
622 Nevertheless, this result not only adds to existing demonstrations of endogenous oscillations entrained
623 by tACS, it also points to entrained neural oscillations being more than just a passive response to
624 rhythmic input. This idea is discussed in detail in the next section.

625

626 *Rhythmic entrainment echoes – active predictions or passive after-effect?*

627 In both our MEG and tACS experiments, we demonstrate that entrained neural and perceptual processes
628 are more than a simple reflection of rhythmic input driving an otherwise silent system (Fig. 7A): Based
629 on the observation of sustained oscillatory responses after stimulus offset, we conclude that an
630 endogenous oscillatory system is involved in such entrained brain responses. Although endogenous
631 oscillations are difficult to measure during stimulation, the most parsimonious explanation of our results
632 is that the entrained response entails both evoked responses and endogenous oscillations, with the former
633 dominating the response. After stimulus offset only the latter prevails, leading to a change in
634 topographical pattern and estimated source. Indeed, we found that sensors capturing sustained

635 oscillations also show a significantly entrained response during sensory stimulation (Fig. 3C, red), while
 636 stronger, stimulus-driven activity at distinct sensors, quickly subsided after stimulation (green in Fig.
 637 3C).



638
 639 **Figure 7. Three physical models that could be invoked to explain neural entrainment, and their potential to explain**
 640 **rhythmic entrainment echoes. A. In a system without any endogenous processes (e.g., neural oscillations), driving input**
 641 **would produce activity which ceases immediately when this input stops. B. A more direct account of rhythmic**
 642 **entrainment echoes is that endogenous neural oscillations resemble the operation of a pendulum which will start**
 643 **swinging passively when “pushed” by a rhythmic stimulus. When this stimulus stops, the oscillation will persist but**
 644 **decays over time, depending on certain “hard-wired” properties (similar to the frictional force and air resistance that**
 645 **slows the movement of a pendulum over time). C. Endogenous neural oscillations could include an active (e.g.,**
 646 **predictive) component that controls a more passive process – similar to a child that can control the movement of a**
 647 **swing. This model predicts that oscillations are upheld after stimulus offset as long as the timing of important upcoming**
 648 **input (dashed lines) can be predicted. Note that, for the sake of clarity, we made extreme predictions to illustrate the**
 649 **different models. For instance, depending on the driving force of the rhythmic input, pendulum and swing could reach**
 650 **their maximum amplitude near-instantaneously in panels B and C, respectively, and therefore initially resemble the**
 651 **purely driven system shown in A. Similarly, it is possible that the predictive process (illustrated in C) operates less**
 652 **efficiently in the absence of driving input and therefore shows a decay similar to that shown by the more passive process**
 653 **(shown in B).**

654
 655 What is the neural mechanism and functional role played by these rhythmic echoes of previously
 656 entrained responses (hereafter, “entrainment echoes”, cf. [54])? We here illustrate two different, but not

657 mutually exclusive, models which can explain the observed entrainment echoes. In one model, these
658 rhythmic echoes reflect the passive reverberation of an endogenous neural oscillation that has previously
659 been activated by a rhythmic stimulus. A physical analogy for this would be a pendulum that responds
660 to a regular “push” by swinging back and forth, and that continues to produce a regular cyclical
661 movement without external input until its kinetic energy has subsided (Fig. 7B). In the other model,
662 stimulus-aligned oscillations are the result of an active mechanism that, through predictive processes,
663 comes to align the optimal (high-excitability) oscillatory phase to the expected timing of important
664 sensory or neural events [12,13]. In this view, oscillatory activity can be actively maintained after
665 stimulus offset and can persist for as long as these predictions are required. It is plausible that this active
666 component is imposed onto a more “hard-wired”, passive mechanism, that is oscillations might be
667 entrained passively, but that this mechanism is under top-down control and can be adjusted if necessary.
668 A physical analogy for this is the way in which a child will move on a swing if pushed, but can also
669 control whether or not the movement of the swing is sustained after their helper stops pushing (Fig. 7C).
670 The active mechanism, in this case, is the timing and amplitude of small movements that a sufficiently
671 skilled child can coordinate with the movement of the swing to maintain oscillations without external
672 help.

673

674 Several of our observations do point to an “active” component involved in generating rhythmic
675 entrainment echoes, however, providing a definitive answer to this question remains for future studies.
676 In both experiments, we found that the neural systems involved in producing sustained effects are
677 distinct from those that are most active during the presence of the rhythmic stimulus. In Experiment 1,
678 sustained MEG oscillations were maximal at parietal sensors and had a clearly different scalp
679 topography and source configuration from typical auditory responses (cf. [46] for a similar shift towards
680 parietal sensors after rhythmic stimulation). In Experiment 2, individual tACS phase lags leading to
681 highest word report accuracy *after* tACS offset were unrelated to those measured *during* tACS.
682 Together, these findings are important as they speak against purely “bottom-up” or stimulus-driven
683 generators of sustained oscillatory responses that merely continue to reverberate for some time after
684 stimulus offset. Instead, they suggest that a distinct oscillatory network seems to be involved that might

685 be specialized in “tracking” and anticipating important upcoming sensory events – potentially by
686 adjusting and modulating a more passive, sensory processing system that aligns to rhythmic speech
687 stimuli. It is possible that we can mimic such top-down effects using tACS, providing rhythmic
688 predictions to auditory regions using electrical stimulation.

689

690 This proposal that top-down predictions for the timing of up-coming stimuli are achieved using neural
691 oscillations is also in line with previous studies suggesting that neural predictions are fundamental for
692 how human speech is processed by the brain [25,63–65]. It is possible that predictive oscillatory
693 mechanisms are particularly strong for intelligible speech, and therefore upheld for some time when the
694 speech stops. In contrast, unintelligible noise-like sequences, typically irrelevant in everyday situations,
695 might lead to weaker predictions or shorter-duration sustained responses – explaining the results
696 observed in Experiment 1.

697

698 Stronger rhythmic responses during intelligible than unintelligible speech [5,6], as well as sustained
699 oscillatory effects for speech sounds [17], have previously been shown in auditory brain areas. However,
700 all of these studies measured neural effects during auditory input, which might bias localization of the
701 neural responses towards auditory areas. Our study, in contrast, revealed sustained effects during post-
702 stimulus silent periods at parietal sensors. This method might therefore yield a more precise estimate of
703 where these effects originate. Auditory input fluctuates rapidly, which requires the auditory system to
704 quickly adapt its oscillations to changes in input [66,67]. Auditory input is represented more faithfully
705 (i.e. less abstractly), and therefore on a faster time scale, in auditory brain regions than in “higher-level”
706 ones [68]. Thus, it is possible that oscillatory activity in the former involves more immediate responses,
707 and hence disappears quickly after sound offset. In contrast, a more abstract representation of a rhythmic
708 input – including phasic predictions about timing – might be more stable over time, and can remain
709 present even after stimulus offset. This might be another reason to explain why our sustained oscillatory
710 effects were found to be maximal at parietal sensors, potentially reflecting neural activity at a higher
711 level of the cortical hierarchy.

712

713 *Predicting tACS outcomes from EEG data – implications for future work and applications*

714 It is a common observation that participants differ in how they respond to a given tACS protocol. For
715 example, there is typically no consistent tACS phase which leads to highest perceptual accuracy for all
716 participants [7–10]. Individualizing brain stimulation protocols has therefore been proposed as a crucial
717 step to advance the theoretical and practical application of this line of research [26–28]. A recent study
718 [69] reported that the phase relation between tACS and visual flicker modulates the magnitude of EEG
719 responses to the flicker when tACS is turned off. Moreover, the individual “best” phase relation between
720 tACS and flicker (leading to strongest EEG responses) was correlated with the individual phase relation
721 between EEG and flicker. We replicate and extend this finding in a new modality by showing that the
722 individual phase lag between EEG and intelligible speech can predict which tACS phase leads to more
723 or less accurate perception in the same participant. Indeed, we found that EEG data from individual
724 participants is sufficient to predict which tACS phase is optimal for perception, so long as the average
725 lag between the two can be estimated even when using other, independent participants (Fig. 6). This
726 result is important, as it shows that tACS can be adapted to individual brains based on EEG observations
727 and establishes a method for aligning EEG and tACS findings for single participants. In an applied
728 setting, these methods make the application of brain stimulation more efficient since the search for the
729 most effective phase can be guided by EEG data rather than by trial and error. This finding therefore
730 increases the potential for clinical or educational applications of tACS methods in future.

731

732 Perhaps surprisingly, given results from Experiment 1, the phase of the entrained, but not sustained EEG
733 response was predictive for the phase of the sustained tACS effect. This result might be explained by
734 the fact that, possibly due the lower signal to noise ratio of EEG, the sustained oscillatory response was
735 not statistically reliable in the EEG in Experiment 1 (Fig. 5A). Consequently, a link between sustained
736 oscillatory effects in EEG and tACS might not have been detectable, even if it exists, simply because
737 the former was not measured reliably. Nevertheless, our finding that the entrained EEG response predicts
738 sustained tACS phase indicates that entrained EEG responses can capture the phase of endogenous
739 oscillations, despite observations of simultaneous evoked neural activity. MEG, showing statistically
740 robust sustained responses (Fig. 2), is not as closely related to tACS as EEG (as its signal is not affected

741 by the same distortions by bone and tissue) and is therefore less likely to be predictive of tACS outcomes
742 (cf. Fig. S3). Future studies may need electrophysiological methods with higher signal to noise ratio
743 than EEG, such as electrocorticography, ECoG, to test the relationship between sustained neural
744 responses and tACS-induced changes in perception in more detail.

745 According to the simplest interpretation of the reciprocity between EEG and tACS, if the signal from a
746 neural source is captured at a certain (EEG) electrode position, then the same electrode position should
747 be efficient in stimulating this neural source (with tACS) [30–32]. Vice versa, if a tACS electrode
748 configuration is successful in targeting a certain neural source, then activity from this source should be
749 measurable with EEG at this electrode position. As the topographical pattern of EEG signals with high
750 predictive value for tACS (fronto-occipital pattern; Fig. 5D) was different from the tACS electrode
751 position (T7/8), our results indicate that this simple interpretation does not hold and that more complex
752 mechanisms underlie our observations. This could be because multiple neural sources are involved and
753 interact to produce the topographical distribution measured with EEG, while the tACS protocol used
754 can only reach one or some of them. It is also possible that tACS modulates the efficacy of sensory input
755 to activate neural ensembles, while EEG measures the output of these ensembles. Differences in neural
756 populations contributing to input vs output processing, including their orientation to the scalp, might
757 explain the observed deviance from simple reciprocity between EEG and tACS. Finally, it is possible
758 that even stronger modulation of perception could be achieved if tACS were applied at those (fronto-
759 occipital) EEG electrode positions showing maximal predictive values for tACS effects – this could be
760 explored in future work.

761 It is of note that the phasic modulation of speech perception was not statistically reliable when the target
762 was presented during tACS (i.e. in the ongoing tACS condition). This result seems in contrast to
763 previous work [7–11]. However, in those studies, participants listened to and reported longer speech
764 sequences while they were asked to detect a single target word (presented in background noise) in the
765 current study. The quasi-regular rhythm of such sequences might act as an additional entraining stimulus
766 which could boost or interact with tACS effects (see also next paragraph), in particular when perception
767 is tested during tACS. Future studies should test the interesting question of whether and how the
768 rhythmicity of the speech stimulus affects the efficacy of tACS during and after its application.

769
770
771
772
773
774
775
776
777
778
779
780
781
782
783
784
785
786
787
788
789
790
791
792
793
794
795
796

In previous work, using the same electrode configuration as applied in Experiment 2, we reported that tACS can only disrupt, and not enhance speech perception [8]. We previously hypothesized that this is because tACS was applied simultaneously with rhythmic speech sequences, which as Experiment 1 of our study shown can themselves entrain brain activity. If neural entrainment to the speech sequences were already at the limit of what is physiologically possible, tACS might only be able to disrupt, but not to enhance it further. Importantly, in the current study, tACS was applied during non-rhythmic background noise, i.e. without any simultaneously entraining auditory stimulus. Our finding of enhanced speech perception therefore supports the hypothesis that tACS can enhance neural entrainment. However, if it is applied simultaneously with a strong “competing” entraining stimulus, tACS might only be able to disrupt entrainment. Together with the finding that tACS can be individualized, the protocol used here seems a promising method for future technological applications in which tACS is used to enhance speech perception in a real-world setting.

In conclusion, we report evidence that endogenous neural oscillations are a critical component of brain responses that are aligned to intelligible speech sounds. This is a fundamental assumption in current models of speech processing [1] that we believe is only now clearly established by empirical evidence. We further show that tACS can modulate speech perception by entraining endogenous oscillatory activity. In this way we believe our work critically advances our understanding of how neural oscillations contribute to the processing of speech in the human brain.

797 **Materials and Methods**

798

799 **Participants**

800 24 participants were tested after giving written informed consent in a procedure approved by the
801 Cambridge Psychology Research Ethics Committee (application number PRE.2015.132) and carried out
802 in accordance with the Declaration of Helsinki. 3 participants did not finish Experiment 1, leaving data
803 from 21 participants (10 females; mean \pm SD, 37 ± 16 years) for further analyses; 4 participants did not
804 finish Experiment 2, leaving 20 participants for further analyses (11 females; 39 ± 15 years). 18
805 participants (9 females; 40 ± 15 years) finished both experiments.

806 All participants were native English speakers, had no history of hearing impairment, neurological
807 disease, or any other exclusion criteria for MEG or tACS based on self-report.

808

809 **Stimuli**

810 Our stimuli consisted of a pool of ~650 monosyllabic words, spoken to a metronome beat at 1.6 Hz
811 (inaudible to participants) by a male native speaker of British English (author MHD). These were time-
812 compressed to 2 and 3 Hz, respectively, using the pitch-synchronous overlap and add (PSOLA)
813 algorithm implemented in the Praat software package (version 6.12). This approach ensures that
814 “perceptual centres”, or “p-centres” [70] of the words were aligned to the metronome beat (see vertical
815 lines in Fig. 1C) and, consequently, to rhythmic speech (in perceptual terms). Moreover, the well-
816 defined rhythmicity of the stimulus allows a precise definition of the phase relation between stimulus
817 and tACS (see below).

818

819 For Experiment 1 (Fig. 1A), these words were combined to form rhythmic sequences, which were 2 or
820 3 seconds long and presented at one of two different rates (2 or 3 Hz). Depending on the duration and
821 rate of the sequence, these sequences therefore consisted of 4 (2 Hz / 2 s), 6 (3 Hz / 2 s and 2 Hz / 3s) or
822 9 words (3 Hz / 3s). Noise-vocoding [18] is a well-established method to produce degraded speech
823 which varies in intelligibility, depending on the number of spectral channels used for vocoding. In
824 Experiment 1, we used highly intelligible 16-channel vocoded speech and 1-channel noise-vocoded

825 speech, which is a completely unintelligible, amplitude-modulated noise (for more details, see [7,8]).
826 Importantly, noise-vocoding does not alter the rhythmic fluctuations in sound amplitude of the stimulus
827 that are commonly assumed to be important for neural entrainment [47]. Thus, acoustic differences in
828 the broadband envelope between the two conditions cannot be responsible for differences in the
829 observed neural responses.

830

831 For Experiment 2 (Fig. 4A), we presented participants with single 16-channel noise-vocoded target
832 words, time-compressed to 3 Hz. These words were embedded in continuous noise with an average
833 spectrum derived from all possible (~650) target words. The noise was presented for ~ 5-7 s. The target
834 word occurred between 2 and 1.722 s before noise offset, depending on its phase lag relative to tACS
835 (see Experimental Design and Fig. 4A). The noise was faded in and out at the beginning and end of each
836 trial, respectively. All stimuli were presented to participants via headphones (through insert earphones
837 connected via tubing to a pair of magnetically-shielded drivers in Experiment 1; ER-2 insert earphones
838 in Experiment 2; Etymotic Research Inc., USA).

839

840 **Experimental Design**

841 In Experiment 1, while MEG/EEG data was recorded, participants listened to the rhythmic sequences
842 (Fig. 1A) and pressed a button as soon as they detected an irregularity in the sequence rhythm (red in
843 Fig. 1A). The irregularity was present in 12.5 % of the sequences and was produced by shifting one of
844 the words (excluding first and last) in the sequence by ± 68 ms. Participants completed 10 experimental
845 blocks of 64 trials each. For each block, the rate of the sequences was chosen pseudo-randomly and kept
846 constant throughout the block. In each trial, the intelligibility (16- or 1-channel speech) and duration (2
847 or 3 s) of the sequence was chosen pseudo-randomly. Consequently, participants completed a total of
848 80 trials for each combination of conditions (rate x intelligibility x duration). Each of the sequences was
849 followed by a silent interval in which sustained oscillatory responses were measured (Fig. 1C). These
850 silent intervals were $2+x$ s long, where x corresponds to 1.5, 2, or 2.5 times the period of the sequence
851 rate (i.e. 0.75, 1, or 1.25 s in 2-Hz blocks, and 0.5, 0.666, or 0.833 s in 3-Hz blocks). x was set to 2 in
852 50 % of the trials.

853 In Experiment 2, tACS was applied at 3 Hz and participants were asked to identify a target word
854 embedded in noise, and report it after each trial using a standard computer keyboard. The start and end
855 of each trial was signaled to participants as the fade in and out of the background noise, respectively
856 (Fig. 4A). The next trial began when participants confirmed their response on the keyboard. We used an
857 intermittent tACS protocol (cf. [69]), i.e. tACS was turned on and off in each trial. In two different tACS
858 conditions, we tested how the timing of the target word relative to tACS modulates accuracy of reporting
859 the target. In both conditions, the target word was presented so that its p-centre occurred at $3+y$, $4+y$, or
860 $5+y$ seconds after tACS onset, chosen pseudo-randomly in each trial (red lines in Fig. 4A). y corresponds
861 to one out of six tested phase delays between tACS and the perceptual center of the target word, covering
862 one cycle of the 3-Hz tACS (corresponding to temporal delays between 66.67 ms and 344.45 ms, in
863 steps of 55.56 ms). In the pre-target tACS condition, tACS was turned off y seconds before the
864 presentation of the target word. In the ongoing tACS condition, tACS remained on during the
865 presentation of the target word and was turned off $1-y$ seconds after target presentation. In each trial, the
866 background noise was faded in with a random delay relative to tACS onset (between 0 and 0.277 s).
867 This ensured that the interval between noise onset and target was unrelated to the phase lag between
868 tACS and target, avoiding potential alternative explanations for the hypothesized phasic modulation of
869 word report by tACS. The background noise was faded out 1.5- y seconds after target presentation.

870

871 Participants completed 10 blocks of 36 trials each, leading to a total of 10 trials for each combination of
872 conditions (tACS condition \times duration \times phase delay). Prior to the main experiment, they completed a
873 short test in which the signal-noise ratio (SNR) between target word and background noise was adjusted
874 and word report accuracy was assessed. During this test, no tACS was applied. Acoustic stimulation
875 was identical to that in the main experiment, apart from the SNR, which was varied between -8 dB and
876 8 dB (in steps of 4 dB; 15 trials per SNR). From this pre-test, a single SNR condition at the steepest
877 point on the psychometric curve (word report accuracy as a function of SNR) was selected and used
878 throughout the main experiment (methods used for quantification of word report accuracy are described
879 below in Quantification and Statistical Analysis). This SNR was, on average -1.05 dB (SD: 1.75 dB).

880 For those participants who completed both experiments, Experiment 1 was always completed prior to
881 Experiment 2, with, on average, 23 days between experiments (std: 30.88 days). However, all but two
882 participants completed both experiments within one week of each other.

883

884 **MEG/EEG Data Acquisition and Pre-processing (Experiment 1)**

885 MEG was recorded in a magnetically and acoustically shielded room, using a VectorView system
886 (Elekta Neuromag) with one magnetometer and two orthogonal planar gradiometers at each of 102
887 positions within a hemispheric array. EEG was recorded simultaneously using 70 Ag-AgCl sensors
888 according to the extended 10–10 system and referenced to a sensor placed on the participant’s nose. All
889 data were digitally sampled at 1 kHz and band-pass filtered between 0.03 and 333 Hz (MEG) or between
890 0.1 and 333 Hz (EEG), respectively. Head position and electrooculography activity were monitored
891 continuously using five head-position indicator (HPI) coils and two bipolar electrodes, respectively. A
892 3D digitizer (FASTRAK; Polhemus, Inc.) was used to record the positions of the EEG sensors, HPI
893 coils, and ~70 additional points evenly distributed over the scalp relative to three anatomical fiducial
894 points (the nasion and left and right preauricular points).

895

896 Data from MEG sensors (magnetometers and gradiometers) were processed using the temporal
897 extension of Signal Source Separation [71] in MaxFilter software (Elekta Neuromag) to suppress noise
898 sources, compensate for motion, and reconstruct any bad sensors.

899 MEG/EEG data were further processed using the FieldTrip software [72] implemented in MATLAB
900 (The MathWorks, Inc.).

901

902 EEG data was high-pass filtered at 1 Hz and re-referenced to the sensor average. Noisy EEG sensors
903 were identified by visual inspection and replaced by the average of neighbouring sensors. For MEG and
904 EEG data separately, artefacts caused by eye movements, blinks, or heartbeat, were extracted using
905 independent component analysis (ICA). ICA was applied to data down-sampled to 150 Hz. ICA
906 components representing artefacts were identified visually and removed from the data at the original

907 sampling rate of 1 kHz. The data were then epoched into trials from -3 s (longer condition) or -2 s
908 (shorter condition) to +2.5 s, relative to the omission of the first word in each sequence (cf. Fig. 1C).

909

910 **Electrical Stimulation (Experiment 2)**

911 Current was administered using two battery-driven stimulators (DC-Stimulator MR, Neuroconn GmbH,
912 Ilmenau, Germany). Each of the stimulators was driven remotely by the output of one channel of a high-
913 quality sound card (Fireface UCX, RME, Germany); another output channel was used to transmit diotic
914 auditory stimuli to the participants' headphones, assuring synchronization between applied current and
915 presented stimuli.

916

917 We used a tACS electrode configuration that has produced a reliable modulation of word report in a
918 previous study [8]. This protocol entails bilateral stimulation over auditory areas using ring electrodes
919 (see inset of Fig. 4A). Each pair of ring electrodes consisted of an inner, circular, electrode with a
920 diameter of 20 mm and a thickness of 1 mm, and an outer, "doughnut-shaped", electrode with an outer
921 and inner diameter of 100 and 75 mm, respectively, and a thickness of 2 mm. The inner electrodes were
922 centered on T7 and T8 of the 10-10 system, respectively. The parts of the outer electrodes which
923 overlapped with participants' ears were covered using electrically isolating tape. Electrodes were kept
924 in place with adhesive, conductive ten20 paste (Weaver and Company, Aurora, CO, USA). Stimulation
925 intensity was set to 1.4 mA (peak-to-peak) unless the participant reported stimulation to be unpleasant,
926 in which case intensity was reduced (consequently, two participants were stimulated with 1.2 mA, one
927 with 1.1 mA, and one with 1.0 mA). Current was not ramped up or down; we verified in preliminary
928 tests that for sinusoidal stimulation this does not lead to increased current-induced sensations.

929

930 Sham stimulation was not applied in this experiment. Sensations produced by tACS are typically
931 strongest at the onset of the electrical stimulation. Based on this notion, during sham stimulation, current
932 is usually ramped up and down within several seconds, leading to similar sensations as during "true"
933 tACS, but with no stimulation in the remainder of the trial or block (e.g., [73]). In the current experiment,
934 we tested whether tACS applied for only several seconds leads to a phasic modulation of perception.

935 Given the similarity of this approach to a typical sham stimulation condition, we did not expect that it
936 would act as an appropriate control. Instead, we compared the observed tACS-induced modulation of
937 speech perception with that obtained in a surrogate distribution, reflecting the null distribution (see
938 Quantification and Statistical Analysis).

939

940 We verified in pre-tests that turning on or off the electric stimulation does not produce any sensation
941 that is temporally so precise that participants can distinguish the two conditions (note that tACS is
942 applied intermittently in both conditions, only with different timings relative to the target word).
943 However, we did not measure potential sensations quantitatively during the experiment to avoid drawing
944 attention to the transient nature of our tACS protocol. However, even if tACS sensations differed
945 between the two conditions at the relevant time points (e.g., during target presentation), they seem
946 unlikely to have affected the hypothesized phasic modulation of word report (for this to happen,
947 participants would also need to distinguish different tACS phases, and relate these phases to the time at
948 which the target is presented; see [8] for further discussion). Rather, we might expect a generic effect of
949 tACS such as a difference in overall word report accuracy (averaged across phase). This result was not
950 observed in the current study and hence we feel confident that the phasic effects of pre-target tACS are
951 due to entrainment of underlying neural mechanisms.

952

953 **Statistical Analyses**

954 All analyses were implemented using custom MATLAB scripts and the toolbox for circular statistics
955 [74], where appropriate.

956

957 *Experiment 1*

958 We first quantified rhythmic responses in our data using inter-trial phase coherence (ITC; Fig. 1D). At
959 a given frequency and time, ITC measures the consistency of phase across trials [75,76]. ITC ranges
960 between 0 (no phase consistency) and 1 (perfect phase consistency). Although some studies used
961 spectral power to quantify oscillatory activity in rhythmic paradigms (e.g., [2]), ITC can be considered
962 more appropriate in our case as it (1) as a measure based on phase, not power, directly takes into account

963 the temporal structure of the data [20] and (2) is less affected by power differences across trials, which
964 can bias results (e.g., trials with disproportionately high power can dominate the outcome). ITC at
965 frequency f and time point t was calculated as follows:

$$966 \quad ITC(f, t) = \left| \frac{1}{N} \sum_{n=1}^N e^{i(\varphi(f, t, n))} \right|$$

967 where $\varphi(f, t, n)$ is the phase in trial n at frequency f and time point t , and N is the number of trials.

968 φ was estimated using Fast Fourier Transform (FFT) in sliding time windows of 1 s (step size 20 ms;
969 shown in grey in Fig. 1C,D), leading to a frequency resolution of 1 Hz. Note that, when the outcome of
970 this time-frequency analysis is displayed (Figs. 1E, 3C, 5A,B,E, 6B), “time” always refers to the center
971 of this time window.

972

973 ITC was calculated separately for each of the 204 orthogonal planar gradiometers and then averaged
974 across the two gradiometers in each pair, yielding one ITC value for each of the 102 sensors positions.

975 Data from magnetometers was only used for source localization (see below).

976

977 Our hypothesis states that we expect stronger rhythmic responses (i.e. ITC) at a given frequency when
978 it corresponds to the rate of the (preceding) stimulus sequence (I and III in Fig. 1E,F) than when it does
979 not (II and IV in Fig. 1E,F). We developed an index to quantify this rate-specificity of the measured
980 brain responses (RSR). An RSR larger than 0 reflects a rhythmic response which follows the stimulation
981 rate:

$$982 \quad RSR_t = (ITC(f = 2, r = 2, t) - ITC(f = 2, r = 3, t)) + \\ 983 \quad (ITC(f = 3, r = 3, t) - ITC(f = 3, r = 2, t))$$

984 where f and r correspond to the frequency for which ITC was determined and sequence rate (both in
985 Hz), respectively. For most analyses, t corresponds to a time interval within which ITC was averaged.

986 Two such intervals were defined (white boxes in Fig. 1E): One to quantify rate-specific responses *during*
987 the sequences, but avoiding sequence onset and offset (-1 to -0.5 s relative to the first omitted word),
988 termed “entrained”. The other to quantify rate-specific responses that *outlast* the sequences, and
989 avoiding their offset (0.5 to 2 s relative to the first omitted word), termed “sustained”.

990

991 To test whether rhythmic responses are present in these time windows and in the different conditions,
992 we compared the RSR against 0, using Student's t-test (one-tailed, reflecting the one-directional
993 hypothesis). We used two-tailed repeated-measures t-tests to compare RSR between intelligible and
994 unintelligible conditions (16-channel vs 1-channel speech, averaged across durations), between shorter
995 and longer sequences (2 s vs 3 s, averaged across intelligibility conditions), and to test for their
996 interaction (by comparing their difference). In experimental designs with two conditions per factor, this
997 approach is equivalent to an ANOVA. For all sensors and conditions (intelligibility, duration) separately,
998 we verified that the RSR is normally distributed ($p > 0.05$ in Kolmogorov-Smirnov test), a pre-requisite
999 for subjecting it to parametric statistical tests. Note that such a behaviour is expected, given the central
1000 limit theorem (combining multiple measures leads to a variable that tends to be normally distributed).
1001 Fig. S5A shows the distribution of RSR, averaged across sensors and conditions. Finally, we constructed
1002 a surrogate distribution to verify that an RSR of 0 indeed corresponds to our null hypothesis. This was
1003 done by adding a random value to the phase in each trial before re-calculating ITC and RSR as described
1004 above, and repeating the procedure 100 times to obtain a simulated distribution of RSR values in the
1005 absence of a rhythmic response. This distribution of RSR values was indeed centred on 0, and its 95%
1006 confidence interval included 0 (Fig. S5B). Once again, this justifies our use of parametric statistical tests
1007 to confirm whether the observed RSR is greater than zero.

1008 Statistical tests were applied separately for each of the 102 MEG sensor positions (i.e. gradiometer pairs;
1009 Fig. 2). Significant RSR (differences) were determined by means of cluster-based permutation tests
1010 (5000 permutations) [77]. Sensors with a p-value ≤ 0.05 were selected as cluster candidates. Clusters
1011 were considered significant if the probability of obtaining their cluster statistic (sum of t-values) in the
1012 permuted dataset was $\leq 5\%$.

1013

1014 Electro- or neurophysiological data analyzed in the spectral domain (e.g., to calculate ITC) often include
1015 aperiodic, non-oscillatory components with a "1/f" shape [23,24]. These 1/f components can bias the
1016 outcome of spectral analyses [23,24]. Although this primarily affects estimates of oscillatory power
1017 (e.g., higher power for lower frequencies), higher power leads to more reliable estimates of phase and

1018 therefore potentially also to higher ITC (even though this measure is analytically independent of power,
1019 see above). 1/f components are also influenced by stimulus input [78]. Consequently, it is possible that
1020 these aperiodic components differ between stimulus rates and therefore affect our RSR. To rule out such
1021 an effect, we repeated our RSR analysis, using ITC values corrected for 1/f components. For this
1022 purpose, a 1/f curve [24] was fitted to the ITC as a function of neural frequency, averaged within the
1023 time window of interest (dashed lines in Fig. 3B, left). This was done separately for each participant,
1024 sensor, stimulus rate, and experimental condition (intelligibility and duration), as these factors might
1025 influence the shape of the aperiodic component. Each of these fits was then subtracted from the
1026 corresponding data; the resulting residuals (Fig. 3B, right) reflect 1/f-corrected ITC values and were
1027 used to calculate RSR as described above. This procedure revealed prominent peaks at neural
1028 frequencies corresponding to the two stimulus rate (Fig. 3B, right), suggesting successful correction for
1029 aperiodic, non-oscillatory components. Given the absence of a pronounced 1/f component in the
1030 entrained time window (Fig. 3A), we here only show results for the sustained time window (Fig. 3B,
1031 Fig. S1).

1032
1033 Participants' sensitivity to detect an irregularity in the stimulus rhythm was quantified using d-prime
1034 (d'), computed as the standardized difference between hit probability and false alarm probability:

$$1035 \quad d' = z(p_{hit}) - z(p_{false\ alarm})$$

1036 where, in a given condition, p_{hit} and $p_{false\ alarm}$ are the probability of correctly identifying an irregular
1037 sequence and falsely identifying a regular sequence as irregular, respectively.

1038
1039 To test whether performance in this task is correlated with rate-specific brain responses during or after
1040 the rhythmic sounds, we selected MEG sensors which responded strongly in the two time windows
1041 defined. In the entrained time window, all sensors were included in a significant cluster revealed by the
1042 analyses described above (Fig. 2C); we therefore selected the 20 sensors with the largest RSR. In the
1043 sustained time window, we selected all sensors which were part of a significant cluster (Fig. 2F). The
1044 RSR from those sensors (averaged within the respective time window) was correlated with performance
1045 (d'), using Pearson's correlation. Even in conditions with relatively weak brain responses, these

1046 can still be related to task performance. For the correlation analysis, we therefore averaged both RSR
1047 and d-prime across conditions (intelligibility, duration, and rate, the latter for d-prime only).

1048

1049 MEG analyses in source space are not necessarily superior to those in sensor space, in particular when
1050 the signal of interest is expected to be relatively weak [79], such as in the current study (rhythmic brain
1051 responses in the absence of sensory stimulation). While sensor space analyses are assumption-free,
1052 reconstruction methods required for transformation to source space all make certain assumptions which
1053 can lead to increased uncertainty if they are invalid [80]. Given that we do not require inferences about
1054 the exact spatial location or extent of the hypothesized sustained oscillations, we focus here on analyses
1055 in sensor space. Nevertheless, we do also report results in source space for completeness, while
1056 emphasizing that they should be, for these reasons, be interpreted with caution.

1057 RSR measured with MEG were source-localized using the following procedure. First, for each
1058 participant, MEG data was co-registered with their individual T1-weighted structural MRI, via
1059 realignment of the fiducial points. A structural MRI scan was not available for one participant, who was
1060 excluded from source analysis. Lead fields were constructed, based on individual MRI scans, using a
1061 single shell head model. Brain volumes were spatially normalized to a template MNI brain, and divided
1062 into grid points of 1 cm resolution. Source reconstruction was then performed, using a linear constrained
1063 minimum variance beamformer algorithm (LCMV [81]). Spatial filters were estimated, one for each of
1064 the two time windows of interest (entrained and sustained), and for each of the two neural frequencies
1065 that contribute to the RSR (2 Hz and 3 Hz). For each spatial filter, data from the two stimulus rates (2
1066 Hz and 3 Hz) was combined, and single trials were band-pass filtered (2nd order Butterworth) at the
1067 frequency for which the filter was constructed (2 Hz filter: 1-3 Hz; 3 Hz filter: 2-4 Hz). Data from
1068 gradiometers and magnetometers was combined. To take into account differences in signal strength
1069 between these sensor types, data from magnetometers was multiplied by a factor of 20 before the
1070 covariance matrix (necessary for LCMV beamforming) was extracted. Using other factors than 20 did
1071 not change results reported here. The spatial filters were then applied to fourier-transformed single-trial
1072 data at the frequency for which the filters were constructed (2 Hz and 3 Hz). The spatially filtered,
1073 fourier-transformed single-trials were then combined to form ITC, using the formula provided above.

1074 For *each* of the two stimulus rates (2 Hz and 3 Hz), this step yielded one ITC value per neural frequency
1075 of interest (2 Hz and 3 Hz), and for each of 2982 voxels inside the brain. These ITC values were then
1076 combined to RSR values, as described above.

1077

1078 *Experiment 2*

1079 Participants' report of the target word was evaluated using Levenshtein distance [82], which is the
1080 minimum number of edits (deletions, insertions etc.) necessary to change a phonological representation
1081 of the participants responses into the phonology of the target word, divided by the number of phonemes
1082 in the word. Accuracy in the task was defined as $1 - \text{Levenshtein distance}$; this measure varies between
1083 0 and 1, where 1 reflects a perfectly reproduced target word (see [25] for details).

1084

1085 For each participant, tACS condition and duration separately, we tested how report accuracy varies with
1086 phase lag (corresponding to the delay between target word and tACS offset in the pre-target tACS
1087 condition, and to the actual tACS phase in the ongoing tACS condition; see Fig. 4A). This was done by
1088 fitting a cosine function to task accuracy as a function of phase lag (Fig. 4D), an approach which has
1089 recently been revealed as highly sensitive at detecting a phasic modulation of perception [21]. The
1090 amplitude of the cosine (a in Fig. 4D) reflects how strongly performance varies as a function of phase
1091 lag. Note that a is always larger than 0. To test statistical significance, we therefore constructed a
1092 surrogate distribution, which consists of amplitude values that would be observed in the absence of the
1093 hypothesized phase effect. For this purpose, phase lags were randomly assigned to trials and the analysis
1094 repeated to these shuffled datasets. This procedure was repeated 1000 times, yielding 1000 amplitude
1095 values for each experimental condition. The surrogate distribution was then compared with the single
1096 outcome obtained from the original, non-permuted data, resulting statistical (z -) values, according to:

$$1097 \quad z = (d - \mu) / \sigma$$

1098 where d is the observed data, and μ and σ are mean and standard deviation of the surrogate distribution,
1099 respectively [21,22].

1100 The phasic modulation of task accuracy, induced by tACS in a given condition, was considered reliable
1101 if the z -value exceeded a critical value (e.g., $z = 1.645$, corresponding to a significant threshold of $\alpha =$

1102 0.05, one-tailed). We first tested for a phasic modulation of word report accuracy, irrespective of tACS
1103 duration (Fig. 4F). For this purpose, data was pooled over tACS duration before the cosine amplitudes
1104 were extracted. We then repeated the cosine fit procedure, separately for each duration (Fig. 4G). We
1105 analyzed the data separately for each tACS condition, as well as for their average. For the latter, cosine
1106 amplitude values were averaged since this does not require a consistent preferred phase for both
1107 conditions. For all statistical tests, values obtained from the surrogate distribution were treated in the
1108 same way as described for the original data.

1109 To evaluate differences in phasic modulation of task accuracy between tACS conditions and durations,
1110 additional surrogate distributions were constructed by randomly assigning the variable of interest (i.e.
1111 tACS condition or tACS duration) to single trials and re-computing cosine amplitudes. To test for
1112 differences between tACS conditions, the difference in cosine amplitude between the two conditions
1113 was compared with the same difference in the surrogate distribution, using z-values as described above
1114 (two-tailed). Likewise, to test for differences between tACS durations, for each tACS condition
1115 separately and for their average, the difference in cosine amplitude between the longest (5-s) and shortest
1116 (3-s) durations was compared with the same difference in the surrogate distribution (one-tailed). To test
1117 for an interaction between tACS condition and duration, we first determined the difference in cosine
1118 amplitude between 5-s and 3-s tACS for each tACS condition, and then compared the difference between
1119 the two conditions with the same difference in the surrogate distribution (two-tailed).

1120

1121 *Experiment 1 vs 2*

1122 Given the expected relationship between tACS and EEG [29–32], we tested whether the phase lag
1123 between tACS and target word, leading to particularly accurate or inaccurate responses in Experiment
1124 2, can be predicted from the phase of EEG responses to rhythmic speech sequences in Experiment 1.

1125 For this purpose, at each time point throughout the trial, EEG phase (φ_{EEG} , green in Fig. 5B-II) was
1126 extracted at 3 Hz (corresponding to the frequency at which tACS was applied in Experiment 2). Note
1127 that φ_{EEG} corresponds to $\varphi(f, t)$ defined above, where $f = 3$ Hz, and phase was averaged across trials
1128 at time point t . As described above, φ was estimated using FFT and sliding analysis windows of 1 s.
1129 φ_{EEG} can therefore be understood as the phase of a 3-Hz cosine fitted to data within this 1-s window

1130 (shaded grey in Fig. 5B-I). The value of φ_{EEG} corresponds to the distance between each of the three
1131 cosine peaks and the end of the corresponding cycle (defined as π ; arrow in Fig. 5B-I).

1132 To obtain a more reliable estimate of phase, we combined phase estimates within each of the two time
1133 windows of interest (entrained and sustained). As averaging φ_{EEG} across time would lead to phase
1134 cancellation effects, we first determined, for each time point, the phase relation (i.e. circular difference)
1135 between EEG and the presented sequences. For the latter, φ_{Sound} (orange in Fig. 5B-II) was defined so
1136 that the perceptual centre of each word corresponds to π (compare example sounds on top of Fig. 5B-I
1137 with φ_{Sound} in Fig. 5B-II). Assuming a rhythmic EEG response that follows the presented sounds, the
1138 phase lag between φ_{EEG} and φ_{Sound} should be approximately constant across time. The circular
1139 difference between the two, labeled $\varphi_{EEGvsSound}$ (Fig. 5B-III) was therefore averaged within each of
1140 the two time windows. For the longer (3-s) sequences in Experiment 1, the entrained time window was
1141 extended to -2 to -0.5 s relative to the first omitted word (-1 to -0.5 s for shorter sequences).

1142

1143 For each the two tACS conditions, the phase of the cosine fitted to individual data, averaged across
1144 durations, was extracted (φ_{tACS} in Fig. 4D). φ_{tACS} reflects the position of the cosine peak (i.e. the
1145 “preferred” tACS phase, leading to highest accuracy), relative to the maximal phase lag tested (here: π).
1146 For each participant, EEG electrode, and combination of conditions in the two experiments, we then
1147 extracted the circular difference between φ_{tACS} (Fig. 4D,E) and $\varphi_{EEGvsSound}$ (Fig. 5B-III,5C-I). The
1148 distribution of this difference (Fig. 5C-II,III) reveals whether there is a consistent phase lag between
1149 φ_{tACS} and $\varphi_{EEGvsSound}$ across participants. In this case, we would expect a non-uniform distribution,
1150 which was assessed with Rayleigh’s test for non-uniformity (Fig. 5D). Despite potential differences in
1151 the *magnitude* of rhythmic brain responses, the different sequence durations tested in Experiment 1
1152 should not differ in their *phase relation* to the sound. The $\varphi_{EEGvsSound}$ obtained in these conditions
1153 were therefore averaged. Finally, we selected 29 EEG sensors whose phase during intelligible speech
1154 was predictive (FDR-corrected $p \leq 0.05$ in Rayleigh’s test) for φ_{tACS} in the pre-target tACS condition
1155 (cf. Fig. 5D). The z-values, obtained from Rayleigh’s test, were averaged and displayed as a function of
1156 time (i.e. not averaged within the two windows as described above).

1157

1158 Although methodologically more distant to tACS than EEG (only the latter two are affected by
1159 distortions by skull and tissue), we repeated the procedure for the simultaneously acquired MEG data
1160 (Fig. S3). Here, to avoid phase cancellation effects, z-values were calculated separately for each of the
1161 204 gradiometers and then averaged across the two gradiometers in each pair, yielding one z-value for
1162 each of the 102 sensors positions (note that z-values from Rayleigh's test are always larger or equal to
1163 0).

1164

1165 We also used the obtained results to re-align behavioural outcomes in Experiment 2 relative to the
1166 predicted optimal tACS phase (leading to highest accuracy) in individual participants. The primary
1167 purpose of this re-alignment is to illustrate implications of results obtained in the analysis described in
1168 the preceding paragraph (Fig. 5D). We also used a leave-one-participant-out procedure to avoid the
1169 inherent circularity in defining preferred phases or phase lags with the same data as used in the eventual
1170 analysis. This procedure is depicted in Fig. 6.

1171 Step 1 (Fig. 6A): For each participant i , data from all remaining participants was used to estimate the
1172 average difference between φ_{tACS} (from the pre-target tACS condition) and $\varphi_{EEGvsSound}$. $\varphi_{EEGvsSound}$
1173 was determined in the entrained time window, at electrode F3 (showing the highest predictive value for
1174 φ_{tACS} in the pre-target condition). Step 2 (Fig. 6B): $\varphi_{EEGvsSound}$ was determined for participant i . Step
1175 3 (Fig. 6C): The $\varphi_{EEGvsSound}$, obtained for participant i in step 2, was shifted by the average difference
1176 between φ_{tACS} and $\varphi_{EEGvsSound}$, obtained in step 1. This yielded the predicted φ_{tACS} for participant i .
1177 Step 4 (Fig. 6D): The predicted φ_{tACS} was used to estimate the tACS phase lag with highest perceptual
1178 accuracy for participant i . This phase lag was calculated as $\pi - \varphi_{tACS}$, based on the fact that φ_{tACS} reflects
1179 the distance between the peak of a fitted cosine and the maximal tACS phase lag (Fig. 4B). The
1180 behavioural data from participant i was then shifted by the predicted optimal phase lag, so that highest
1181 accuracy was located at a centre phase bin. As behavioural data was only available for six different
1182 phase lags, it was (linearly) interpolated between these data points (167 interpolated values between
1183 each phase lag) to enable a more accurate re-alignment of the data (note that the predicted φ_{tACS} depends
1184 on (1) the phase of the cosine fitted to individual data and (2) $\varphi_{EEGvsSound}$, neither of which are
1185 restricted to the six phase values tested). Step 5 (Fig. 6E): Steps 1-4 were repeated, separately for each

1186 of the 18 participants. Step 6 (Fig. 6F). The re-aligned data was averaged across participants, with the
1187 hypothesis of highest accuracy at the predicted optimal phase lag for word report accuracy. This
1188 hypothesis was tested by comparing accuracy at this phase lag (0 in Fig. 6F) with accuracy at the one
1189 180° (or π) away, using a one-tailed (given the clear one-directional hypothesis) paired t-test.

1190

1191 In a final analysis, we used this re-alignment procedure to test whether a modulation of perception during
1192 or after tACS reflects enhancement or disruption of perception (or both). As our experimental protocol
1193 prevented the inclusion of the usual sham stimulation condition (see Electrical Stimulation), we based
1194 this analysis on the finding that φ_{tACS} was not reliably predicted by $\varphi_{EEGvsSound}$ in the ongoing tACS
1195 condition. We repeated the procedure described in the preceding paragraph; however, we used it to re-
1196 align behavioral outcome from the ongoing tACS condition to the phase lag predicted to be optimal for
1197 word report accuracy. Consequently, the only difference to the procedure described above is the use of
1198 φ_{tACS} obtained in the ongoing (not pre-target) tACS condition.

1199

1200 We compared accuracy at the predicted optimal tACS phase lag between the two tACS conditions.
1201 Given that $\varphi_{EEGvsSound}$ is not predictive for φ_{tACS} in the ongoing tACS condition, any tACS-dependent
1202 changes in perception should be abolished by the re-alignment procedure, and the outcome reflects the
1203 null hypothesis. Consequently, higher accuracy at the predicted optimal phase lag in the pre-target tACS
1204 condition indicates an enhancement of speech perception, produced by tACS. This was tested by means
1205 of a one-tailed (given the clear one-directional hypothesis) paired t-test. Finally, we repeated the
1206 alignment procedure for both conditions, but this time aligned the behavioural data at the predicted worst
1207 phase lag for speech perception (i.e. 180° or π away from the predicted optimal phase). Again, we
1208 compared accuracy at this predicted worst phase lag between the two tACS conditions, using a one-
1209 tailed repeated-measures t-test. Lower accuracy at the predicted worst phase lag in the pre-target tACS
1210 condition indicates a disruption of speech perception, produced by tACS.

1211

1212 **Data and Software Availability**

1213 Data and custom-built MATLAB scripts are available (<https://osf.io/xw8c4/>).

1214

1215 **Acknowledgements**

1216 The authors thank Isobella Allard for support during pilot testing, Loes Beckers and Clare Cook for help
1217 with data acquisition, and Anne Kösem, Nina Suess and Nathan Weisz for advice on MEG source
1218 localization.

1219

1220 **References**

- 1221 1. Giraud A-L, Poeppel D. Cortical oscillations and speech processing: emerging computational principles
1222 and operations. *Nat Neurosci.* 2012;15: 511–517. doi:10.1038/nn.3063
- 1223 2. Ding N, Melloni L, Zhang H, Tian X, Poeppel D. Cortical tracking of hierarchical linguistic structures in
1224 connected speech. *Nat Neurosci.* 2016;19: 158–164. doi:10.1038/nn.4186
- 1225 3. Peelle JE, Davis MH. Neural Oscillations Carry Speech Rhythm through to Comprehension. *Front*
1226 *Psychol.* 2012;3: 320. doi:10.3389/fpsyg.2012.00320
- 1227 4. Zoefel B, VanRullen R. The Role of High-Level Processes for Oscillatory Phase Entrainment to Speech
1228 Sound. *Front Hum Neurosci.* 2015;9: 651. doi:10.3389/fnhum.2015.00651
- 1229 5. Peelle JE, Gross J, Davis MH. Phase-locked responses to speech in human auditory cortex are enhanced
1230 during comprehension. *Cereb Cortex.* 2013;23: 1378–1387. doi:10.1093/cercor/bhs118
- 1231 6. Gross J, Hoogenboom N, Thut G, Schyns P, Panzeri S, Belin P, et al. Speech rhythms and multiplexed
1232 oscillatory sensory coding in the human brain. *PLoS Biol.* 2013;11: e1001752.
1233 doi:10.1371/journal.pbio.1001752
- 1234 7. Zoefel B, Archer-Boyd A, Davis MH. Phase Entrainment of Brain Oscillations Causally Modulates Neural
1235 Responses to Intelligible Speech. *Curr Biol.* 2018;28: 401-408.e5. doi:10.1016/j.cub.2017.11.071
- 1236 8. Zoefel B, Allard I, Anil M, Davis MH. Perception of Rhythmic Speech Is Modulated by Focal Bilateral
1237 Transcranial Alternating Current Stimulation. *J Cogn Neurosci.* 2020;32: 226–240.
1238 doi:10.1162/jocn_a_01490
- 1239 9. Riecke L, Formisano E, Sorger B, Başkent D, Gaudrain E. Neural Entrainment to Speech Modulates
1240 Speech Intelligibility. *Curr Biol.* 2018;28: 161-169.e5. doi:10.1016/j.cub.2017.11.033
- 1241 10. Wilsch A, Neuling T, Obleser J, Herrmann CS. Transcranial alternating current stimulation with speech
1242 envelopes modulates speech comprehension. *NeuroImage.* 2018;172: 766–774.
1243 doi:10.1016/j.neuroimage.2018.01.038
- 1244 11. Keshavarzi M, Kegler M, Kadir S, Reichenbach T. Transcranial alternating current stimulation in the theta
1245 band but not in the delta band modulates the comprehension of naturalistic speech in noise. *NeuroImage.*
1246 2020;210: 116557. doi:10.1016/j.neuroimage.2020.116557
- 1247 12. Lakatos P, Karmos G, Mehta AD, Ulbert I, Schroeder CE. Entrainment of neuronal oscillations as a
1248 mechanism of attentional selection. *Science.* 2008;320: 110–113. doi:10.1126/science.1154735
- 1249 13. Schroeder CE, Lakatos P. Low-frequency neuronal oscillations as instruments of sensory selection. *Trends*
1250 *Neurosci.* 2009;32: 9–18. doi:10.1016/j.tins.2008.09.012
- 1251 14. Obleser J, Kayser C. Neural Entrainment and Attentional Selection in the Listening Brain. *Trends Cogn*
1252 *Sci.* 2019;23: 913–926. doi:10.1016/j.tics.2019.08.004

- 1253 15. Zoefel B. Speech Entrainment: Rhythmic Predictions Carried by Neural Oscillations. *Curr Biol.* 2018;28:
1254 R1102–R1104. doi:10.1016/j.cub.2018.07.048
- 1255 16. Zoefel B, ten Oever S, Sack AT. The Involvement of Endogenous Neural Oscillations in the Processing of
1256 Rhythmic Input: More Than a Regular Repetition of Evoked Neural Responses. *Front Neurosci.* 2018;12.
1257 doi:10.3389/fnins.2018.00095
- 1258 17. Kösem A, Bosker HR, Takashima A, Meyer A, Jensen O, Hagoort P. Neural Entrainment Determines the
1259 Words We Hear. *Curr Biol.* 2018;28: 2867–2875.e3. doi:10.1016/j.cub.2018.07.023
- 1260 18. Shannon RV, Zeng FG, Kamath V, Wygonski J, Ekelid M. Speech recognition with primarily temporal
1261 cues. *Science.* 1995;270: 303–304.
- 1262 19. Cousineau D. Confidence intervals in within-subject designs: A simpler solution to Loftus and Masson’s
1263 method. *Tutor Quant Methods Psychol.* 2005; 42–45.
- 1264 20. Rajendran VG, Schnupp JWH. Frequency tagging cannot measure neural tracking of beat or meter. *Proc
1265 Natl Acad Sci.* 2019;116: 2779–2780. doi:10.1073/pnas.1820020116
- 1266 21. Zoefel B, Davis MH, Valente G, Riecke L. How to test for phasic modulation of neural and behavioural
1267 responses. *NeuroImage.* 2019;202: 116175. doi:10.1016/j.neuroimage.2019.116175
- 1268 22. VanRullen R. How to Evaluate Phase Differences between Trial Groups in Ongoing Electrophysiological
1269 Signals. *Front Neurosci.* 2016;10. doi:10.3389/fnins.2016.00426
- 1270 23. Cole SR, Voytek B. Brain Oscillations and the Importance of Waveform Shape. *Trends Cogn Sci.*
1271 2017;21: 137–149. doi:10.1016/j.tics.2016.12.008
- 1272 24. Haller M, Donoghue T, Peterson E, Varma P, Sebastian P, Gao R, et al. Parameterizing neural power
1273 spectra. *bioRxiv.* 2018; 299859. doi:10.1101/299859
- 1274 25. Sohoglu E, Davis MH. Perceptual learning of degraded speech by minimizing prediction error. *Proc Natl
1275 Acad Sci.* 2016;113: E1747–E1756. doi:10.1073/pnas.1523266113
- 1276 26. Romei V, Thut G, Silvanto J. Information-Based Approaches of Noninvasive Transcranial Brain
1277 Stimulation. *Trends in Neurosciences.* 2016: 782–795.
- 1278 27. Zoefel B, Davis MH. Transcranial electric stimulation for the investigation of speech perception and
1279 comprehension. *Lang Cogn Neurosci.* 2017;32: 910–923. doi:10.1080/23273798.2016.1247970
- 1280 28. Kasten FH, Duecker K, Maack MC, Meiser A, Herrmann CS. Integrating electric field modeling and
1281 neuroimaging to explain inter-individual variability of tACS effects. *Nat Commun.* 2019;10: 1–11.
1282 doi:10.1038/s41467-019-13417-6
- 1283 29. Wagner S, Lucka F, Vorwerk J, Herrmann CS, Nolte G, Burger M, et al. Using reciprocity for relating the
1284 simulation of transcranial current stimulation to the EEG forward problem. *NeuroImage.* 2016;140: 163–
1285 173. doi:10.1016/j.neuroimage.2016.04.005
- 1286 30. Helmholtz H. Ueber einige Gesetze der Vertheilung elektrischer Ströme in körperlichen Leitern mit
1287 Anwendung auf die thierisch-elektrischen Versuche. *Ann Phys.* 1853;165: 211–233.
1288 doi:10.1002/andp.18531650603
- 1289 31. Dmochowski JP, Koessler L, Norcia AM, Bikson M, Parra LC. Optimal use of EEG recordings to target
1290 active brain areas with transcranial electrical stimulation. *NeuroImage.* 2017;157: 69–80.
1291 doi:10.1016/j.neuroimage.2017.05.059
- 1292 32. Fernández-Corazza M, Turovets S, Luu P, Anderson E, Tucker D. Transcranial Electrical
1293 Neuromodulation Based on the Reciprocity Principle. *Front Psychiatry.* 2016;7: 87.
1294 doi:10.3389/fpsy.2016.00087

- 1295 33. Shahin AJ, Roberts LE, Miller LM, McDonald KL, Alain C. Sensitivity of EEG and MEG to the N1 and
1296 P2 Auditory Evoked Responses Modulated by Spectral Complexity of Sounds. *Brain Topogr.* 2007;20:
1297 55–61. doi:10.1007/s10548-007-0031-4
- 1298 34. Riecke L, Zoefel B. Conveying Temporal Information to the Auditory System via Transcranial Current
1299 Stimulation. *Acta Acustica United with Acustica.* 2018; 104: 883-886. doi:info:doi/10.3813/AAA.919235
- 1300 35. Walter VJ, Walter WG. The central effects of rhythmic sensory stimulation. *Electroencephalogr Clin
1301 Neurophysiol.* 1949;1: 57–86. doi:10.1016/0013-4694(49)90164-9
- 1302 36. Keitel C, Quigley C, Ruhnau P. Stimulus-driven brain oscillations in the alpha range: entrainment of
1303 intrinsic rhythms or frequency-following response? *J Neurosci.* 2014;34: 10137–10140.
1304 doi:10.1523/JNEUROSCI.1904-14.2014
- 1305 37. Capilla A, Pazo-Alvarez P, Darriba A, Campo P, Gross J. Steady-state visual evoked potentials can be
1306 explained by temporal superposition of transient event-related responses. *PLoS One.* 2011;6: e14543.
1307 doi:10.1371/journal.pone.0014543
- 1308 38. Haegens S, Zion Golumbic E. Rhythmic facilitation of sensory processing: A critical review. *Neurosci
1309 Biobehav Rev.* 2018;86: 150–165. doi:10.1016/j.neubiorev.2017.12.002
- 1310 39. Doelling KB, Assaneo MF, Bevilacqua D, Pesaran B, Poeppel D. An oscillator model better predicts
1311 cortical entrainment to music. *Proc Natl Acad Sci.* 2019; 201816414. doi:10.1073/pnas.1816414116
- 1312 40. Spaak E, de Lange FP, Jensen O. Local entrainment of α oscillations by visual stimuli causes cyclic
1313 modulation of perception. *J Neurosci.* 2014;34: 3536–3544. doi:10.1523/JNEUROSCI.4385-13.2014
- 1314 41. de Graaf TA, Gross J, Paterson G, Rusch T, Sack AT, Thut G. Alpha-band rhythms in visual task
1315 performance: phase-locking by rhythmic sensory stimulation. *PLoS One.* 2013;8: e60035.
1316 doi:10.1371/journal.pone.0060035
- 1317 42. Mathewson KE, Prudhomme C, Fabiani M, Beck DM, Lleras A, Gratton G. Making waves in the stream
1318 of consciousness: entraining oscillations in EEG alpha and fluctuations in visual awareness with rhythmic
1319 visual stimulation. *J Cogn Neurosci.* 2012;24: 2321–2333. doi:10.1162/jocn_a_00288
- 1320 43. Lakatos P, Musacchia G, O’Connell MN, Falchier AY, Javitt DC, Schroeder CE. The spectrotemporal
1321 filter mechanism of auditory selective attention. *Neuron.* 2013;77: 750–761.
1322 doi:10.1016/j.neuron.2012.11.034
- 1323 44. Hickok G, Farahbod H, Saberi K. The Rhythm of Perception: Entrainment to Acoustic Rhythms Induces
1324 Subsequent Perceptual Oscillation. *Psychol Sci.* 2015;26: 1006–1013. doi:10.1177/0956797615576533
- 1325 45. Constantino FC, Simon JZ. Dynamic cortical representations of perceptual filling-in for missing acoustic
1326 rhythm. *Sci Rep.* 2017;7: 1–10. doi:10.1038/s41598-017-17063-0
- 1327 46. Bouwer FL, Fahrenfort JJ, Millard SK, Slagter HA. A silent disco: Persistent entrainment of low-
1328 frequency neural oscillations underlies beat-based, but not memory-based temporal expectations. *bioRxiv.*
1329 2020; 2020.01.08.899278. doi:10.1101/2020.01.08.899278
- 1330 47. Ghitza O. The theta-syllable: a unit of speech information defined by cortical function. *Front Psychol.*
1331 2013;4: 138. doi:10.3389/fpsyg.2013.00138
- 1332 48. Zion Golumbic EM, Ding N, Bickel S, Lakatos P, Schevon CA, McKhann GM, et al. Mechanisms
1333 underlying selective neuronal tracking of attended speech at a “cocktail party.” *Neuron.* 2013;77: 980–
1334 991. doi:10.1016/j.neuron.2012.12.037
- 1335 49. Lakatos P, O’Connell MN, Barczak A, Mills A, Javitt DC, Schroeder CE. The leading sense: supramodal
1336 control of neurophysiological context by attention. *Neuron.* 2009;64: 419–430.
1337 doi:10.1016/j.neuron.2009.10.014

- 1338 50. Hughes HC, Darcey TM, Barkan HI, Williamson PD, Roberts DW, Aslin CH. Responses of Human
1339 Auditory Association Cortex to the Omission of an Expected Acoustic Event. *NeuroImage*. 2001;13:
1340 1073–1089. doi:10.1006/nimg.2001.0766
- 1341 51. Sohoglu E, Chait M. Detecting and representing predictable structure during auditory scene analysis. King
1342 AJ, editor. *eLife*. 2016;5: e19113. doi:10.7554/eLife.19113
- 1343 52. Raij T, Mäkelä JP, McEvoy L, Hari R. Human auditory cortex is activated by omissions of auditory
1344 stimuli. *Int J Psychophysiol*. 1997;25: 73. doi:10.1016/S0167-8760(97)85548-1
- 1345 53. SanMiguel I, Saupe K, Schröger E. I know what is missing here: electrophysiological prediction error
1346 signals elicited by omissions of predicted "what" but not "when". *Front Hum Neurosci*. 2013;7.
1347 doi:10.3389/fnhum.2013.00407
- 1348 54. Stonkus R, Braun V, Kerlin JR, Volberg G, Hanslmayr S. Probing the causal role of prestimulus
1349 interregional synchrony for perceptual integration via tACS. *Sci Rep*. 2016;6: 1–13.
1350 doi:10.1038/srep32065
- 1351 55. Herrmann CS, Rach S, Neuling T, Strüber D. Transcranial alternating current stimulation: a review of the
1352 underlying mechanisms and modulation of cognitive processes. *Front Hum Neurosci*. 2013;7.
1353 doi:10.3389/fnhum.2013.00279
- 1354 56. Antal A, Herrmann CS. Transcranial Alternating Current and Random Noise Stimulation: Possible
1355 Mechanisms. *Neural Plast*. 2016;2016: 3616807. doi:10.1155/2016/3616807
- 1356 57. Pikovsky A. Synchronization: Universal Concept: A Universal Concept in Nonlinear Sciences. 1st
1357 Paperback Ed edition. Cambridge: Cambridge University Press; 2008.
- 1358 58. Ali MM, Sellers KK, Fröhlich F. Transcranial alternating current stimulation modulates large-scale
1359 cortical network activity by network resonance. *J Neurosci*. 2013;33: 11262–11275.
1360 doi:10.1523/JNEUROSCI.5867-12.2013
- 1361 59. Fröhlich F. Experiments and models of cortical oscillations as a target for noninvasive brain stimulation.
1362 *Prog Brain Res*. 2015;222: 41–73. doi:10.1016/bs.pbr.2015.07.025
- 1363 60. Vosskuhl J, Strüber D, Herrmann CS. Non-invasive Brain Stimulation: A Paradigm Shift in Understanding
1364 Brain Oscillations. *Front Hum Neurosci*. 2018;12. doi:10.3389/fnhum.2018.00211
- 1365 61. Notbohm A, Kurths J, Herrmann CS. Modification of Brain Oscillations via Rhythmic Light Stimulation
1366 Provides Evidence for Entrainment but Not for Superposition of Event-Related Responses. *Front Hum
1367 Neurosci*. 2016;10: 10. doi:10.3389/fnhum.2016.00010
- 1368 62. Thut G, Veniero D, Romei V, Miniussi C, Schyns P, Gross J. Rhythmic TMS causes local entrainment of
1369 natural oscillatory signatures. *Curr Biol*. 2011;21: 1176–1185. doi:10.1016/j.cub.2011.05.049
- 1370 63. Blank H, Davis MH. Prediction Errors but Not Sharpened Signals Simulate Multivoxel fMRI Patterns
1371 during Speech Perception. *PLoS Biol*. 2016;14. doi:10.1371/journal.pbio.1002577
- 1372 64. Norris D, McQueen JM, Cutler A. Prediction, Bayesian inference and feedback in speech recognition.
1373 *Lang Cogn Neurosci*. 2016;31: 4–18. doi:10.1080/23273798.2015.1081703
- 1374 65. Davis M, Sohoglu E. Three functions of prediction error for Bayesian inference in speech perception.
1375 Gazzaniga M, Mangun R, & Poeppel D (Eds) *The Cognitive Neurosciences*, 6th Edition. Camb, MA,
1376 USA: MIT Press; 2020.
- 1377 66. Zoefel B, VanRullen R. Oscillatory Mechanisms of Stimulus Processing and Selection in the Visual and
1378 Auditory Systems: State-of-the-Art, Speculations and Suggestions. *Front Neurosci*. 2017;11.
1379 doi:10.3389/fnins.2017.00296
- 1380 67. VanRullen R, Zoefel B, Ilhan B. On the cyclic nature of perception in vision versus audition. *Philos Trans
1381 R Soc Lond B Biol Sci*. 2014;369: 20130214. doi:10.1098/rstb.2013.0214

- 1382 68. Edwards E, Chang EF. Syllabic (~2-5 Hz) and fluctuation (~1-10 Hz) ranges in speech and auditory
1383 processing. *Hear Res.* 2013;305: 113–134. doi:10.1016/j.heares.2013.08.017
- 1384 69. Fiene M, Schwab BC, Misselhorn J, Herrmann CS, Schneider TR, Engel AK. Phase-specific manipulation
1385 of rhythmic brain activity by transcranial alternating current stimulation. *Brain Stimulat.* 2020;13: 1254–
1386 1262. doi:10.1016/j.brs.2020.06.008
- 1387 70. Morton J, Marcus S, Frankish C. Perceptual Centers (P-centers). *Psychol Rev.* 1976; 405–408.
- 1388 71. Taulu S, Simola J, Kajola M. Applications of the signal space separation method. *IEEE Trans Signal*
1389 *Process.* 2005;53: 3359–3372. doi:10.1109/TSP.2005.853302
- 1390 72. Oostenveld R, Fries P, Maris E, Schoffelen J-M. FieldTrip: Open source software for advanced analysis of
1391 MEG, EEG, and invasive electrophysiological data. *Comput Intell Neurosci.* 2011;2011: 156869.
1392 doi:10.1155/2011/156869
- 1393 73. Kasten FH, Dowsett J, Herrmann CS. Sustained Aftereffect of α -tACS Lasts Up to 70 min after
1394 Stimulation. *Front Hum Neurosci.* 2016;10. doi:10.3389/fnhum.2016.00245
- 1395 74. CircStat: A MATLAB Toolbox for Circular Statistics | Berens | *Journal of Statistical Software.* [cited 21
1396 Jun 2017]. Available: <https://www.jstatsoft.org/article/view/v031i10>
- 1397 75. Lachaux JP, Rodriguez E, Martinerie J, Varela FJ. Measuring phase synchrony in brain signals. *Hum*
1398 *Brain Mapp.* 1999;8: 194–208.
- 1399 76. Makeig S, Debener S, Onton J, Delorme A. Mining event-related brain dynamics. *Trends Cogn Sci.*
1400 2004;8: 204–210. doi:10.1016/j.tics.2004.03.008
- 1401 77. Maris E, Oostenveld R. Nonparametric statistical testing of EEG- and MEG-data. *J Neurosci Methods.*
1402 2007;164: 177–190. doi:10.1016/j.jneumeth.2007.03.024
- 1403 78. He BJ. Scale-free brain activity: past, present and future. *Trends Cogn Sci.* 2014;18: 480–487.
1404 doi:10.1016/j.tics.2014.04.003
- 1405 79. Jaiswal A, Nenonen J, Stenroos M, Gramfort A, Dalal SS, Westner BU, et al. Comparison of beamformer
1406 implementations for MEG source localization. *NeuroImage.* 2020;216: 116797.
1407 doi:10.1016/j.neuroimage.2020.116797
- 1408 80. Wendel K, Väisänen O, Malmivuo J, Gencer NG, Vanrumste B, Durka P, et al. EEG/MEG Source
1409 Imaging: Methods, Challenges, and Open Issues. *Comput Intell Neurosci.* 2009; doi:10.1155/2009/656092
- 1410 81. Van Veen BD, van Drongelen W, Yuchtman M, Suzuki A. Localization of brain electrical activity via
1411 linearly constrained minimum variance spatial filtering. *IEEE Trans Biomed Eng.* 1997;44: 867–880.
1412 doi:10.1109/10.623056
- 1413 82. Levenshtein VI. Binary Codes Capable of Correcting Deletions, Insertions and Reversals. SPhD. 1966;10:
1414 707.
- 1415
- 1416
- 1417
- 1418
- 1419
- 1420

1421

1422 **SUPPORTING INFORMATION**

1423 **van Bree et al., Sustained neural rhythms reveal endogenous oscillations supporting speech**
1424 **perception**

1425

1426

1427 **Data S1.** Excel spreadsheet containing, in separate sheets, the underlying numerical data for Figure
1428 panels 1B, 2A-F, 3A-C, 4E-G, 5A,C-E, 6F-G, S1A-D, S2, S3, S5A.

1429

1430

1431

1432

1433

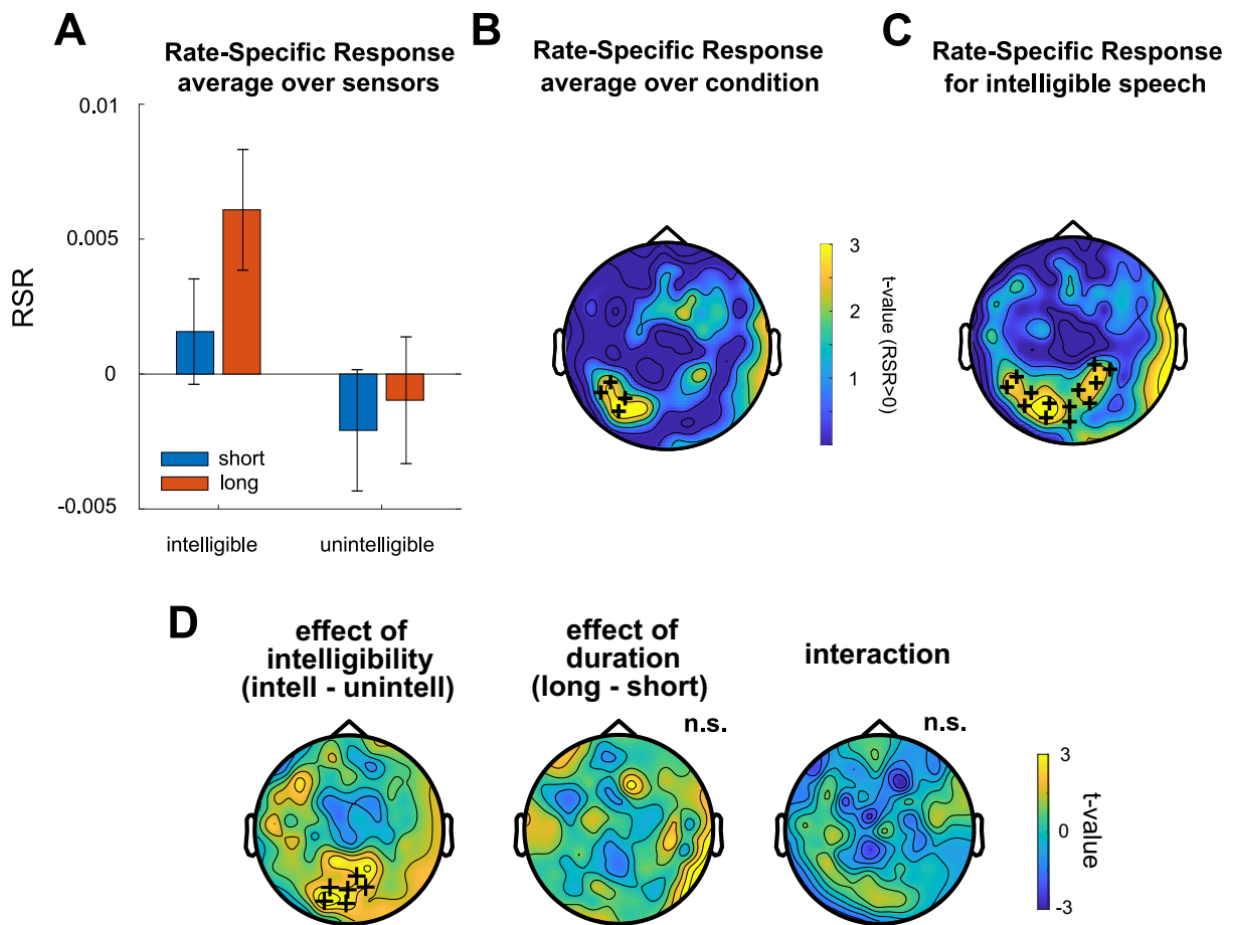
1434

1435

1436

1437

1438



1440

1441

1442 **Figure S1. Rate-specific responses (RSR) in sustained time window after correction for 1/f**
 1443 **component.** Same as in Fig. 2D-F, but using 1/f-corrected Inter-Trial Coherence (shown in Fig. 3B) to
 1444 calculate RSR. Same conventions as for Fig. 2. Please refer to Data S1 for the numerical values
 1445 underlying this figure.

1446

1447

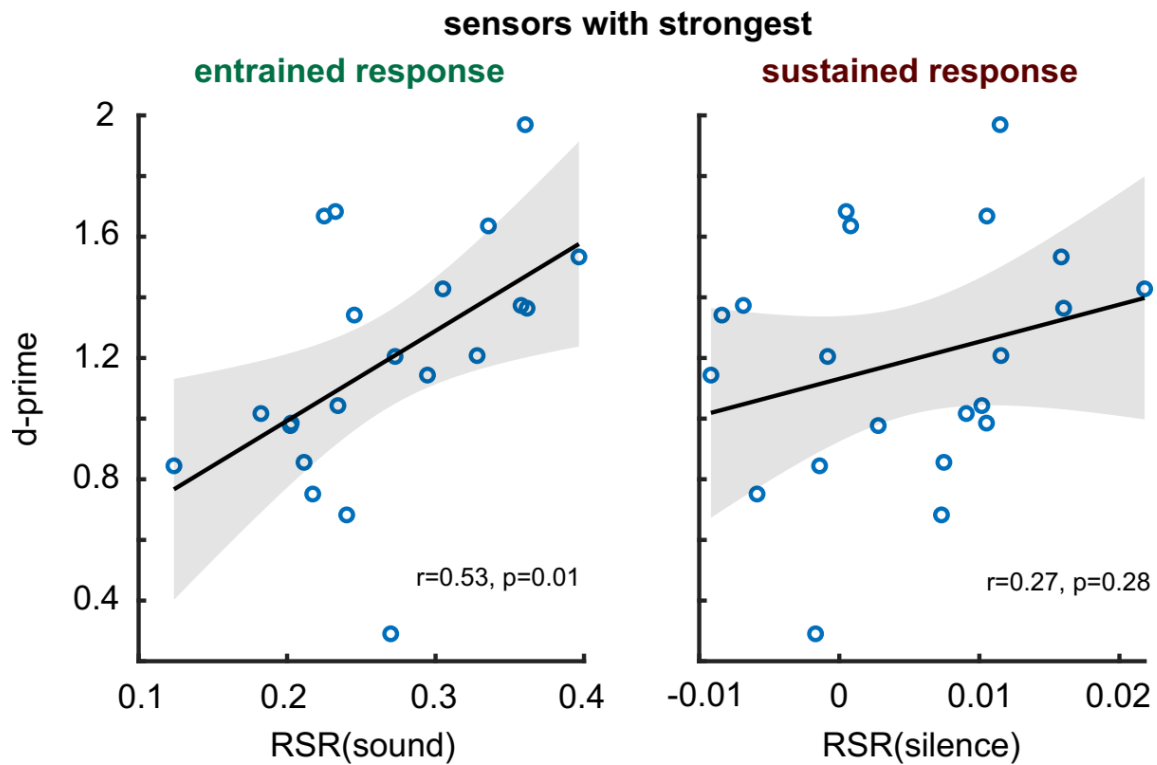
1448

1449

1450

1451

1452



1454 **Figure S2.** Correlation between RSR in the entrained (left) and sustained (right) time windows (for
 1455 the selected sensors shown in Fig. 2C,F), respectively, and performance in the irregularity
 1456 detection task (cf. Fig. 1B). Both RSR and performance were averaged across intelligibility and
 1457 duration conditions; in addition, performance was averaged across rates. Shaded areas correspond to the
 1458 confidence intervals of the regression lines. Please refer to Data S1 for the numerical values underlying
 1459 this figure.

1460

1461

1462

1463

1464

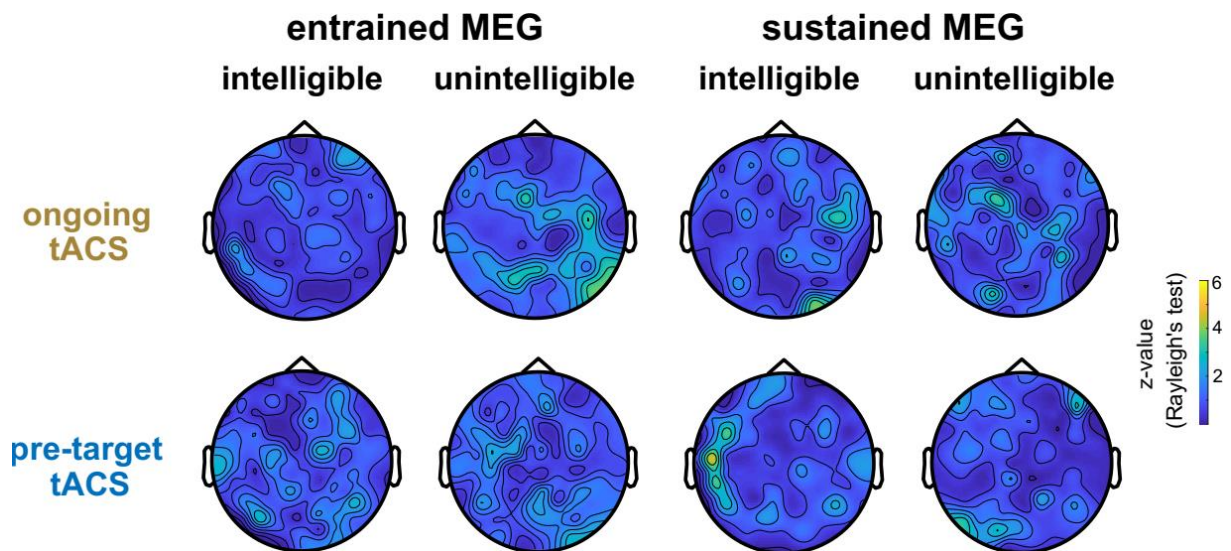
1465

1466

1467

1468

1469



1470

1471 **Figure S3. Using MEG responses to predict optimal tACS phase.** Same as Fig. 5D, but using MEG
 1472 instead of EEG data from Experiment 1. Please refer to Data S1 for the numerical values underlying this
 1473 figure.

1474

1475

1476

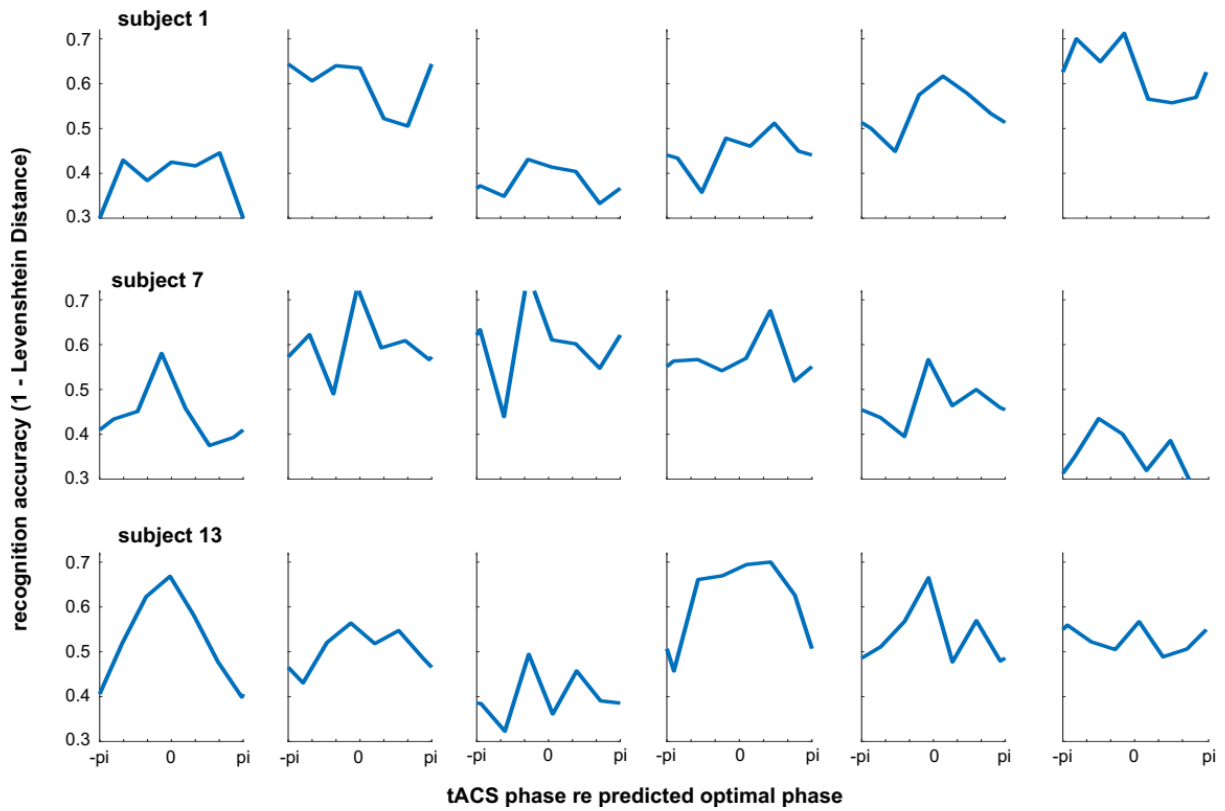
1477

1478

1479

1480

1481



1482

1483 **Figure S4. Data from all individual participants, re-aligned to predicted optimal tACS phase.** Same
 1484 as Fig. 6D,E, but for all 18 participants who were included in the analysis. Note that the average across
 1485 participants is shown in Fig. 6F.

1486

1487

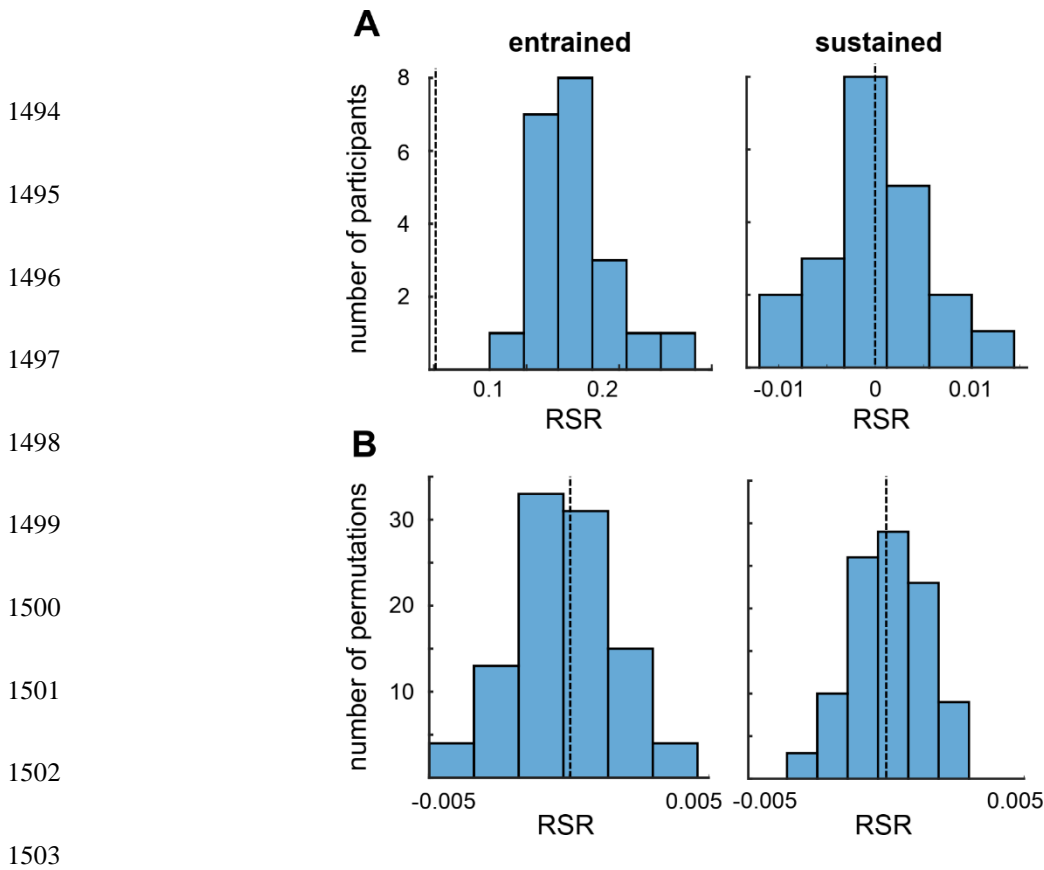
1488

1489

1490

1491

1492



1504 **Figure S5. Control analyses validating RSR as an appropriate measure to reveal rate-specific**
 1505 **rhythmic brain responses.** **A.** Distribution of RSR over participants. Note the approximate normal
 1506 distribution as required for parametric tests (e.g., t-test against 0). Please refer to Data S1 for the
 1507 numerical values underlying this figure panel. **B.** Distribution of RSR, averaged across participants, in
 1508 a surrogate dataset (see Materials and Methods). RSR is centred on 0 (dashed lines), validating our null
 1509 hypothesis of $RSR = 0$. For all results shown here, RSR values have been averaged across sensors and
 1510 conditions (corresponding to the average RSR shown in Fig. 2A,D), including those for which the RSR
 1511 is not reliably different from 0. Statistically significant rate-specific responses after intelligible speech
 1512 are shown in Fig. 2F. Note that x-axes are not identical across panels.